

# Probing excitation/ionization processes in millisecond-pulsed glow discharges in argon through the addition of nitrogen

Glen P. Jackson, Fred L. King\*

*Department of Chemistry, P.O. Box 6045, West Virginia University, Morgantown, WV 26506-6045, USA*

Received 24 June 2002; accepted 31 October 2002

---

## Abstract

The addition of N<sub>2</sub> to a millisecond-pulsed glow discharge (PGD) allows diagnostic measurements of the PGD but is found to drastically influence the transient signals arising from the argon and sputtered analyte atoms. Penning excitation between metastable argon atoms and ground state nitrogen molecules and charge transfer between argon ions and the added nitrogen reduce the degree of ionization of sputtered atoms during the power-on, plateau, period by a factor of ~10 (at 1% N<sub>2</sub> by vol.). The added nitrogen affects sputtered atom emission signals less at this time because electron excitation dominates the excitation of these species. Upon power termination, afterpeak, the added nitrogen prevents plasma recombination in two major mechanisms: (i) the nitrogen reduces the number of argon ions available for recombination in the afterpeak; and (ii) vibrationally excited states of nitrogen slow the thermalization of electrons thereby decreasing recombination efficiency. The argon ion population contributes significantly to the afterpeak increase in the number of metastable argon atoms. These atoms are essential for the afterpeak ionization of sputtered atoms. Judicious selection of the nitrogen partial pressure can tune the delay time of afterpeak ionization/recombination by up to 200 μs. This could be particularly beneficial for time-resolved optical or mass spectrometric analyses.

© 2002 Elsevier Science B.V. All rights reserved.

*Keywords:* Pulsed glow discharge; Argon; Nitrogen; Ionizing plasma; Recombining plasma; Metastable quenching; Excitation/ionization processes; Glow discharge mass spectrometry

---

## 1. Introduction

Glow discharge mass spectrometry (GDMS) is a reliable technique for the bulk and trace analysis of conducting and non-conducting solids [1–9]. Unique analytical advantages are imparted by the dominant mechanisms of analyte ionization that sustain the glow discharge plasma. The ability to

optimize the analytical performance of GDMS depends on an improved understanding of the fundamental processes underlying the atomization/excitation/ionization of analytes. Although analytical discharges operate in relatively pure environments of an inert gas, typically argon, various atmospheric contaminant gases can be present that will influence plasma processes and analyte signals.

Whereas the impact of water vapor on glow discharge mass spectrometry (GDMS) ion signals

---

\*Corresponding author. Tel.: +1-304-293-3435; fax: +1-304-293-4904.

*E-mail address:* fking@wvu.edu (F.L. King).

is well known [10–16], the effect of nitrogen—the main constituent of atmospheric gas—is less well known. Wagatsuma and co-workers [17–19] have studied the effects of  $N_2$  and other gases [20–22], in GD optical emission spectroscopy (GD-OES), but their work did not extend as extensively to mass spectrometric studies [17]. The object of this study is to understand the effect of nitrogen on various plasma processes, and the effect on analyte ion signals in GDMS.

These studies also explore the use of nitrogen as a diagnostic tool to probe plasma processes and characteristics. For example, observation of the rovibrational emission spectrum provides a rotational temperature, which is a good indication of the gas temperature [23,24]. Collisions between  $N_2$  molecules and metastable argon atoms result in the population of specific vibrational states of  $N_2$  [25–29]. Emissions from these vibrational states reflect the relative populations of the two metastable levels at 11.55 and 11.72 eV [26,28].

Careful examination of the ionized species in argon glow discharge mass spectrometry revealed the importance of the metastable states of the discharge gas in ionization processes [30]. The fact that copper ion signals (determined by mass spectrometry) scaled linearly with the product of the copper atom and metastable neon atom populations [determined by atomic absorbance spectroscopy (AAS)] provided considerable evidence for the importance of Penning ionization [31]. A great wealth of research supports the observations of Coburn and Kay—that the metastable atoms are responsible for a large proportion of the sputtered atom ionization in steady-state GDMS [32,33].

Microsecond [34–36] and millisecond [37–43] pulsed glow discharges (PGDs) have provided enhanced ionization efficiencies, and analyte ion signals temporally resolved from the discharge gas species (usually argon). This latter benefit is also highly dependent on the Penning ionization of sputtered atoms following termination of the plasma sustaining voltage [44]. In pulsed glow discharges, power termination enables the electrons to thermalize via elastic collisions with the bath gas [45]. This thermalization of electrons favors their participation in the capture-radiative-cascade (CRC) responsible for the enhancement of meta-

stable atom populations that lead to the afterpeak or afterglow observed in these pulsed glow discharges [46–48]. This has been demonstrated by quenching experiments using methane to prevent the metastable atoms from taking part in the afterpeak processes [49].

The present studies focus on the effects of small quantities of molecular nitrogen in an argon PGD, with emphasis given to the effect on ionization and resulting MS analysis. Optical experiments elucidate many of the effects of  $N_2$  addition on ion and excited-state formation—especially in the recombining afterpeak—and are applicable to GD-OES and GD-AAS analyses as well. Time of flight mass spectrometry (ToF-MS) provides insight into the role of metastable argon atoms on analyte signals and persistent signals such as  $ArH^+$ ,  $Ar_2^+$  and  $Ar^{2+}$ .

## 2. Experimental

### 2.1. Glow discharge

A 4.5-cm diameter iron disk (SRM 1767, NIST, Gaithersburg, MD) served as the cathode sample throughout these experiments. Before taking data, a pre-sputtering time of  $\sim 30$  min ensured the removal of oxide/impurity residues from the cathode surface. Before this pre-sputtering period, the six-way cross was pumped down to below  $10^{-4}$  torr for several hours. The ultra high purity argon (Airgas) was not further purified before use. Water impurities are assumed to be in the range of 10 ppm. A leak valve (Granville Phillips, Boulder, CO) controlled the addition of nitrogen to the plasma. A pressure gauge (Hastings, Hampton VA) measured the partial pressure of nitrogen before and after each experiment. A second leak valve enabled the controlled addition of UHP argon to generate a total pressure of 0.8 torr. Unless otherwise stated the nitrogen partial pressure equaled 0.01 torr ( $\sim 1\%$  by vol.). Discharge operating power was provided by a system consisting of an electrical chopper (GRX 3000, DEI, Fort Collins, CO) that modulated a DC power supply (OPS-3500, Kepco, Flushing, NY). The electrical chopper uses a square wave produced by a frequency generator (DS 345, Stanford Research Systems,

Sunnyvale, CA) to modulate the voltage. This pulsed voltage system provides a square-wave with rise and fall times less than 45 ns.

## 2.2. Optical spectrometry systems

The optical spectrometry system used in these studies has been described previously [41,42,50]. Temporal emission measurements were obtained at a fixed wavelength, by monitoring the output of the photomultiplier tube with a digital oscilloscope (9370 M, Lecroy) while the monochromator was held at a constant wavelength. The output of the photomultiplier tube was fed into a boxcar integrator (EG&G PAR 4121B, Princeton, NJ) as the monochromator was scanned to yield temporally resolved emission spectra. The monochromator and boxcar were synchronized so that the boxcar integrated a 1- $\mu$ s gate width of signal from 10 consecutive pulses before the monochromator scanned to the next position. The boxcar therefore captures at least two data points per position of the grating. The gate could be shifted to any delay time from the onset of the glow discharge pulse to obtain only the emission spectra emitted during the 1- $\mu$ s window at that delay time. This data acquisition setup is therefore able to monitor the emission lines of many different species at a specific time in the plasma. Temporal absorption measurements were obtained as described previously using a lock-in-amplifier (EG&G PAR 5210, Princeton, NJ) linked to the chopper of the incident light beam to provide the oscilloscope with a signal [51].

## 2.3. Time-of-flight mass spectrometry (ToF-MS) system

The pulsed glow discharge time-of-flight mass spectrometry system employed in these investigations is described elsewhere [43]. Operating parameters are given in Table 1. The packet of ions to be analyzed in the flight tube is extracted at right angles to the incident ion beam of the ion extraction lenses. This allows mass spectra to be collected at different times throughout the pulse cycle. A digital delay generator (4144, EG&G, Princeton Applied Research, Princeton, NJ) provided the

Table 1  
Settings used for the PGD-ToF-MS experiments

|                           |                         |
|---------------------------|-------------------------|
| <i>Pressure (torr)</i>    |                         |
| GD source                 | 0.8                     |
| Ion exit plate—skimmer    | $\sim 4 \times 10^{-4}$ |
| Flight tube               | $\sim 5 \times 10^{-6}$ |
| <i>Glow discharge</i>     |                         |
| Peak current              | 0.4 mA                  |
| Peak voltage              | -960 V                  |
| Pulse length              | 5.0 ms                  |
| Ion exit orifice          | 1.0 mm                  |
| Skimmer cone orifice      | 1.0 mm                  |
| <i>TOF</i>                |                         |
| R; Repeller plate         |                         |
| Bias                      | -8.5 V                  |
| Pulse width               | 2 $\mu$ s               |
| Pulse voltage             | +200 V                  |
| E; Extraction plate       | 0 V                     |
| A; Accelerator plate,     |                         |
| flight tube, grid, X2, Y2 | -1500 V                 |
| X1                        | -1850 V                 |
| Y1                        | -1550 V                 |
| Detector                  | -1700 V                 |

delayed extraction pulses and was triggered by the same function generator that creates the glow-discharge pulse. Used in combination with the digital recording oscilloscope this arrangement enabled mass spectra to be obtained at selected temporal intervals with respect to the pulse trigger, in a similar manner described for the emission spectra above.

## 3. Results and discussion

### 3.1. Bath gas temperature measurements

In the present study, the rotational temperature of  $N_2^+$  in a millisecond-pulsed glow discharge is determined for a 0.8-torr argon plasma with  $\sim 1\%$   $N_2$  (vol.). The emission spectrum obtained for the first negative band of  $N_2^+$  ( $B^2\Sigma_u^+ \rightarrow X^2\Sigma_g^+$ ) is shown in Fig. 1a. This spectrum is a time-averaged spectrum. The monochromator was scanned at 0.05-nm increments with an integration time of 0.5 s per point so the emission intensity measured at each wavelength was integrated over approximately 25 pulse cycles. Following the methodology provided by Harrison and co-workers [23,24], the peak intensities of the even *R* branch of lines

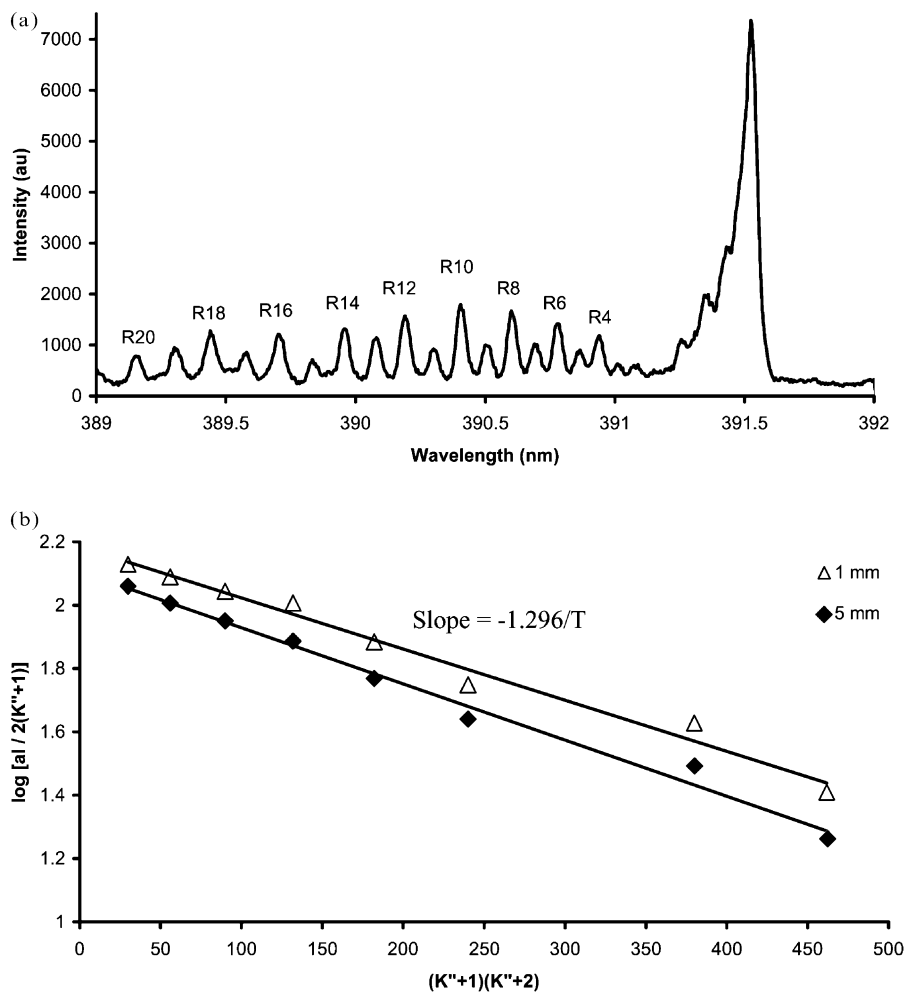


Fig. 1. (a) Time-averaged emission spectrum of the first negative column of  $N_2^+$  in a PGD. Spectrum shown was taken at 5 mm above the cathode surface. (b) Boltzmann plot for the determination of  $T_{rot}$  from the emission spectrum. One percent  $N_2$  in 0.8-torr Ar, 1.5-W peak power.

were used to generate a Boltzmann plot of  $aI/2(K''+1)$  vs.  $(K''+1)(K''+2)$ , as demonstrated in Fig. 1b, where  $a$  is the constant 2 for the even numbers of  $R$ ,  $I$  is the intensity of the line and  $K''$  is the rotational quantum number. The slope of this line is equal to  $-Bhc/kT_{rot}$  where  $B$  is the rotational constant of the vibrational level,  $h$  is Planck's constant,  $c$  is the speed of light,  $k$  is the Boltzmann constant and  $T_{rot}$  is the rotational temperature. Substituting in the values of the con-

stants, the slope is equal to  $-1.296/T_{rot}$ , giving a temperature of 730 K at 5 mm above the cathode. The temperature reaches a maximum of 850 K at a distance 1 mm from the cathode surface. This temperature is considerably higher than the largest rotational temperatures reported previously (of 500–600 K) [23]. However, this study uses a larger pulse power than the previous study, and a lower nitrogen partial pressure. It has been shown that partial pressure of nitrogen can have a signif-

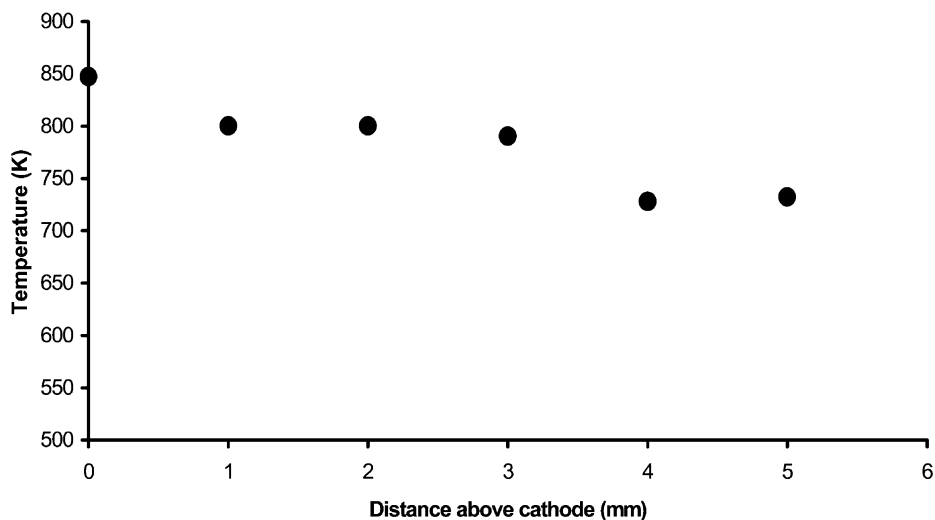


Fig. 2. Time-averaged rotational temperatures in the PGD determined from the emission spectra of  $N_2^+$  as a function of distance above the cathode. One percent  $N_2$  in 0.8-torr Ar, 1.5-W peak power.

ificant effect on the temperature measurements (with higher temperatures measured at lower partial pressures of  $N_2$ ) [24].

A boxcar integrator, used in conjunction with the monochromator as described in Section 2, provided spectra from which time resolved temperature measurements could be obtained. Emission spectra collected before 2 ms and after 5 ms did not contain sufficient signal intensity to be able to calculate reliable temperatures. Between 2 and 5 ms the temperatures were not significantly different from the time-averaged spectra of 720–850 K. Gas temperatures in the prepeak time regime could not be determined using this approach because it actually takes  $>2$  ms for the vibrational levels of  $N_2$  to equilibrate with the gas temperature at the pulse onset [52].

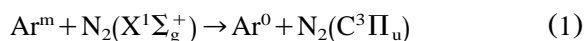
Fig. 2 shows the time-averaged rotational temperature calculated at different distances above the cathode. It is found that the gas temperature decreases as the distance from the cathode increases, consistent with previous findings [23,24]. Two factors contribute to the increased temperature near the cathode: (i) argon ions accelerate across the cathode fall and charge exchange with argon atoms to create fast argon atoms; and (ii) the sputtering

process releases fast atoms and ions [2,8]. These two effects generate atoms and ions with elevated kinetic energies and subsequent elastic collisions efficiently re-distribute this energy to the bulk plasma atoms, thereby increasing the temperature. Because these two methods of kinetic energy deposition are cathode-region specific, the gas temperature is greater here than elsewhere.

In steady-state GDs it is also possible for the cathode to resistively heat as the current flows through the sample. The increased cathode temperature provides another method for the gas near the cathode to acquire additional kinetic energy. In the PGD, the cathode does not heat up as much (this is one benefit of pulsing the discharge) because the discharge is only on for a fraction of the time and the cathode cools between pulses.

### 3.2. $N_2$ quenching of metastable argon atoms

Considerable research has shown [25–29] that electronic energy can be exchanged between the metastable states of argon and the electronic ground state of  $N_2$  in the reaction



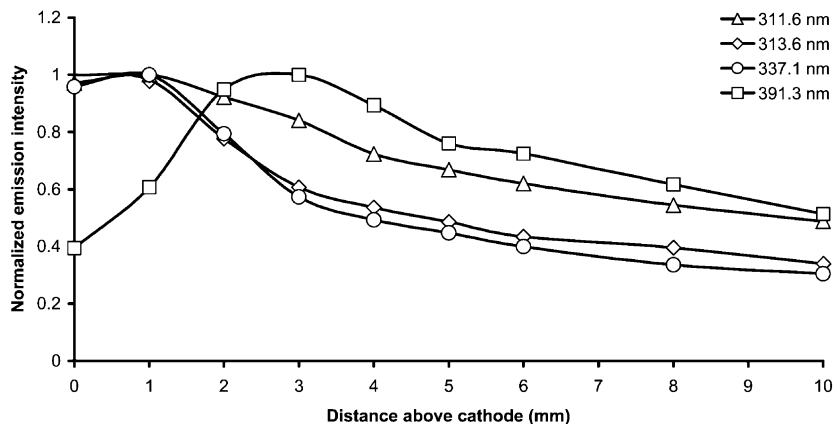


Fig. 3. Comparison of different nitrogen molecular emissions as a function of distance above the cathode. One percent  $N_2$  by volume in 0.8-torr Ar, 5-ms pulse width, 25% duty cycle,  $\sim 1.5$ -W peak power.

The electronically excited nitrogen molecule can also be vibrationally and rotationally excited in this reaction. Indeed, the rovibrational emission spectrum for emissions arising from the  $C^3\Pi_u$  band (not shown) showed rotationally excited states of considerably higher quantum numbers than is observed in Fig. 1 for the excited  $N_2^+$  emissions. Both metastable argon states can populate the  $v'=0,1,2$  vibrational levels, but only the  $^3P_0$  metastable state, at sufficient collision energy, can populate the  $v'=3$  vibrational level [26,28]. The reaction rate for Eq. (1) is  $\sim 3.0 \times 10^{-11} \text{ cm}^3 \text{ s}^{-1}$  for the  $^3P_2$  state [29,53–56] and  $\sim 1.6 \times 10^{-11} \text{ cm}^3 \text{ s}^{-1}$  for the  $^3P_0$  state [55,57]. Although the quenching rate of metastable atoms by  $N_2$  is not particularly fast compared to other small molecules—the quenching rate for water is an order of magnitude faster [57]—the number density of  $N_2$ ,  $\sim 3 \times 10^{14} \text{ cm}^{-3}$  ( $8 \times 10^{-3}$  torr), gives quenching rates in the order of  $\sim 10^4 \text{ s}^{-1}$ . At typical number densities [58,59] of  $Ar^m$  of  $\sim 10^{11} \text{ cm}^{-3}$  (without quenching),  $[N_2] \gg [Ar^m]$  and the metastable atoms should be efficiently quenched.

The excited molecular products undergo radiative relaxation with lifetimes of the second positive transitions ( $C^3\Pi_u \rightarrow B^3\Pi_g$ ) in the order of 40 ns [60,61]. Given the number density of  $N_2$  and a bath gas temperature of  $\sim 800$  K, Penning excitation of the nitrogen molecule will result in emis-

sions from the nascent  $C^3\Pi_u$  products of  $N_2$  before collisional mixing, or rovibrational relaxation can occur [25,28,54].

Several methods exist to verify that excited states of  $N_2$  are formed via Penning excitation in the discharge, and not by fast atom or electron excitation. Two of the most distinguishing factors are (i) that the  $v'=0$  vibrational level of the  $C^3\Pi_u$  manifold will be overpopulated with respect to the Frank–Condon probability factors in the presence of metastable atoms; and (ii) that the rotational fine structure of the  $v'=0$  will extend up to  $K' \approx 49$ , independent of temperature. Also, because the metastable argon states cannot populate nitrogen levels above the  $v'=3$  level, emissions from these levels will not be observable.

As discussed above, the rotational emission spectrum of the (0,0) band of second positive emission with the band head at 337.1 nm showed considerable rotational excitement. The extensive excitation of higher rotational levels is clear evidence for the transfer of energy from metastable states of argon. Emissions from vibrational levels  $>v'=3$  were not observed, also supporting the idea that the excited states are formed predominantly by Penning excitation.

Fig. 3 compares the steady-state emissions of the band-heads for various nitrogen molecular emissions as a function of distance above the cathode. The (0,0) and (2,1) band heads at 337.1

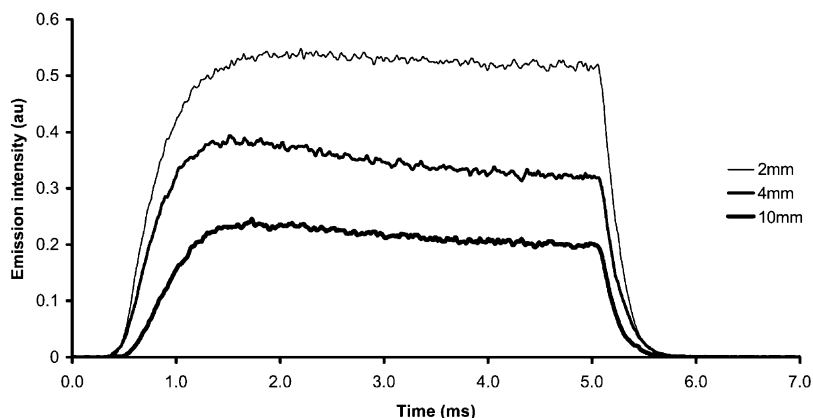


Fig. 4. Temporal emission profiles at 337.1 nm for the (0,0) band of the second positive column. One percent  $N_2$  by volume in 0.8-torr Ar, 5-ms pulse width, 25% duty cycle,  $\sim 1.5$ -W peak power.

and 313.6 nm, respectively, show very similar behavior with an emission maximum near the cathode surface. These values are self-consistent with energy transfer from the metastable atom population that also maximizes at the cathode surface [32,33,51,62]. The (3,2) band emission, corresponding to energy transfer from the  $^3P_0$  metastable state (or possibly the resonant  $^3P_1$  state) is less intense at the cathode surface relative to the negative glow region. This difference could reflect differences in the relative distributions of the metastable states, but because energy transfer from the resonant  $^3P_1$  state cannot be ruled out, this conclusion cannot be verified. The molecular ion emission at 391.3 nm shows considerably different behavior, having a maximum at the edge of the negative glow, at 2–3 mm, and a minimum at the cathode surface. This level lies above the IP of argon, so the only mechanism of populating this state is via electron excitation. Because emissions from the second positive band show such different behavior, this again is verification that the  $C^3\Pi_u$  level is populated predominantly by the metastable atoms.

### 3.3. Effects of $N_2$ on afterpeak ion–electron recombination

It is well known that the afterpeak period of the PGD is CRC-like in behavior [63]. The fundamen-

tal characteristic of the CRC plasma is the downward flow in energy from ion and excited states to the ground-state atoms. The switch from an ionizing plasma to a recombining plasma causes a population inversion and, because of the relatively low electron densities in these conditions, the decay process is predominantly radiative. Although the CRC ultimately ceases at the ground state levels, it is possible for the decay process to pause at the metastable levels because spin-selection rules disallow their decay to the ground state. This is one reason why removal of the plasma-sustaining voltage ordinarily increases the number density of metastable states.

Fig. 4 provides an example of the temporal emission profile at 337.1 nm for the (0,0) band of the second positive transition. Notice that there is no afterpeak increase in the emission for this line, even though one would expect the metastable atom density to increase in afterpeak. Previous work showed that recombination is an effective way of increasing the number density of metastable atoms in the afterpeak period [51]. The decay rates measured in these experiments for the second positive transitions are only marginally slower than for the first negative transitions of the nitrogen molecular ion. If the nitrogen molecules quenched the metastable atoms after they formed, the decay rate for the second positive system should be considerably longer than the first negative system

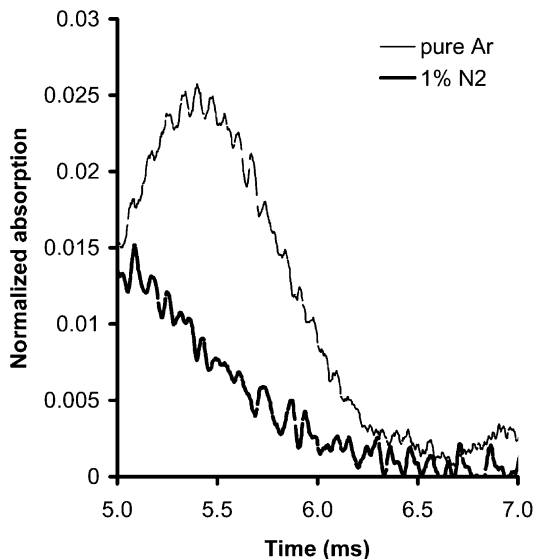


Fig. 5. Effect of nitrogen on the afterpeak population of the  $^3\text{P}_2$  metastable state of argon. Steady-state values have been normalized to the same value at 5.0 ms.

of the  $\text{N}_2^+$  ion. Therefore, it is clear that the nitrogen must be *preventing* metastable atom formation in the afterpeak—not simply quenching

them after they form. Because a large portion of the afterpeak metastable atom population is formed via capture-radiative-cascade (CRC), experiments were performed to discern the effect of  $\text{N}_2$  on the afterpeak processes.

Absorption measurements of the  $^3\text{P}_2$  metastable state at 811.5 nm revealed that the afterpeak increase in metastable atoms normally observed in pure argon PGDs is not observed with 1%  $\text{N}_2$  present. Fig. 5 demonstrates this effect for the region 6 mm above the cathode. Closer to the cathode, afterpeak increases in metastable atoms are not observed in pure argon, so nitrogen did not affect the decay rate of the metastable atoms in this region.

The absorption measurements show that there is no afterpeak increase in metastable atoms when nitrogen is present, which explains why no afterpeak increase is observed for the second positive transition of  $\text{N}_2$ . It should be noted that although deconvoluted data are shown in Fig. 5 the process does not completely remove the effects of the RC time constants [51]. The afterpeak maximum therefore appears more quickly than shown by the data.

Fig. 6 shows the afterpeak/steady-state absorption ratio of the  $^3\text{P}_2$  metastable atom populations

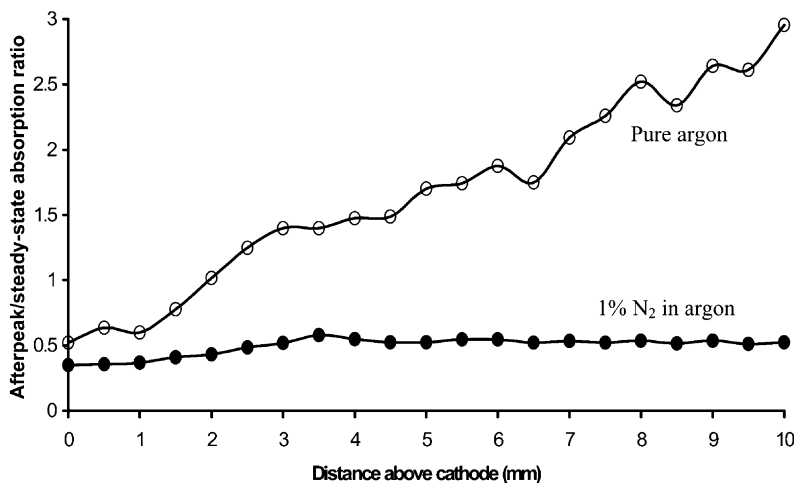


Fig. 6. Plot of the afterpeak/steady-state absorption ratios for the  $^3\text{P}_2$  metastable state of argon, with (filled markers) and without (open markers) the addition of 1%  $\text{N}_2$  to the 0.8-torr argon plasma. Population ratios determined by absorption at 811.5 nm, pulse length 5.0 ms, 0.8-torr Ar,  $\sim 1.5$ -W peak power, Fe cathode.

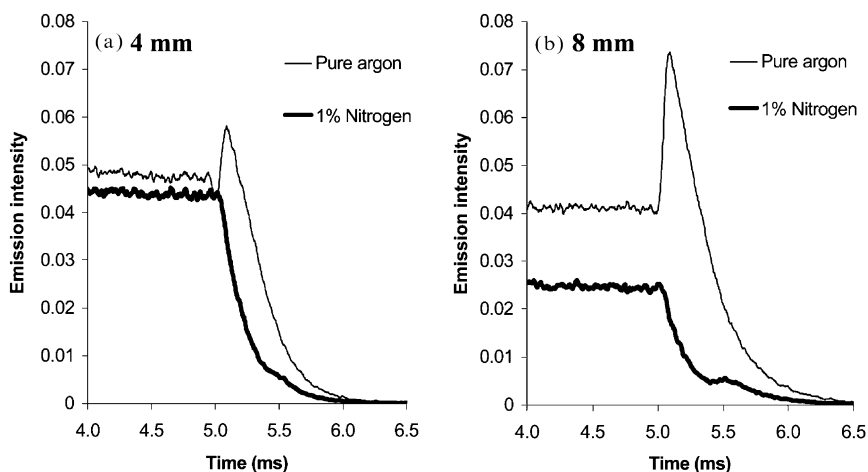


Fig. 7. Emission intensity at 811.5 nm at (a) 4 mm and (b) 8 mm vs. time to show the effect of nitrogen on the afterpeak emissions in an argon PGD. Pulse length: 5.0 ms, 25% duty cycle, 0.8-torr Ar,  $\sim 1.5$ -W peak power, Fe cathode.

plotted as a function of distance above the cathode. The relative populations were determined in a 'pure' argon discharge, and with 1%  $N_2$  added. When no afterpeak increase is observed, the absorption measurement at 5.5 ms is used. This is the time at which afterpeak signals reach a maximum. A ratio greater than one, as seen for the  $^3P_2$  state in pure argon, indicates an afterpeak increase in the population. Both metastable states show an increase in the afterpeak/steady-state ratio as increasing distances from the cathode, but, as observed previously [51] for the copper/argon plasma the afterpeak/steady-state ratios for the  $^3P_2$  states are considerably larger than the  $^3P_0$  state.

When nitrogen is admitted, there is no afterpeak increase in the number of metastable atoms, as shown in Fig. 5, and the ratio remains close to 0.5 at each sampling point. This shows that the decay rate is approximately equal at each distance, although the time constant inherent in the absorption measurements could mask any small changes in decay rates.

The absorption measurements in Figs. 5 and 6 show the effective removal of metastable atoms from the afterpeak, but these measurements do not reveal the exact nature of quenching, i.e. whether the metastable atoms are quenched after they are

formed, and/or if the metastable atom formation is prevented. As alluded to above, the  $N_2$  emissions indicate that metastable atoms are prevented from forming rather than quenched once they are formed. Examination of the afterpeak emissions arising from different excited neutral atoms provides insight into the dominant afterpeak quenching mechanism.

Careful analysis shows that the added nitrogen deleteriously affects, and in fact prevents, the CRC process; thereby yielding an entirely different afterpeak outcome. Fig. 7a,b shows the effect of 1% nitrogen on the afterpeak emission at 811.5 nm at 4 and 8 mm above the cathode, respectively. This emission corresponds to a  $4p-4s$  transition ( $2p_9-1s_5$ ) and leads to the formation of the  $^3P_2$  metastable state. At 4 mm, 1% nitrogen has very little effect on the steady-state population of the upper  $4p$  state, as demonstrated by the similar emission intensities between 4 and 5 ms. Close to the cathode, the electron and fast atom collisions populating and depopulating the  $4p$  (and  $4s$ ) states are fast and outweigh any depopulation caused by the nitrogen. Further from the cathode, at 8 mm for example (Fig. 7b), the steady-state populations of the  $4p$  states are partially quenched by the added nitrogen. This is because excitation and de-

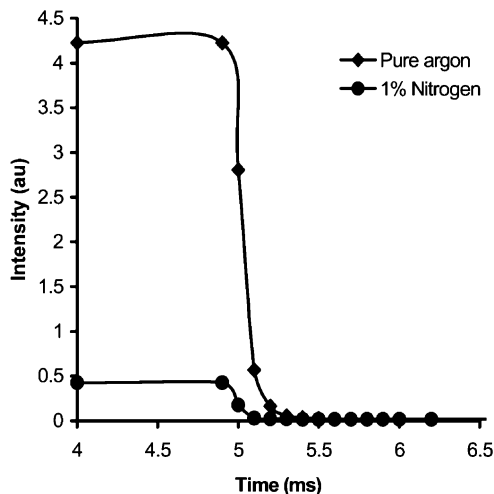


Fig. 8. Argon ion signal at  $m/z=40$  vs. time to show the effect of nitrogen on the steady-state and afterpeak number densities. Sampling orifice positioned at 5 m above the cathode, conditions given above.

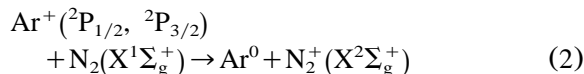
excitation rates are slightly slower here, and step-wise electron excitation via the metastable states is more prominent [64]. Therefore, electronic energy transfer from excited argon states to nitrogen states is more noticeable here.

Fig. 7a,b shows that when the voltage is removed from the pure argon plasma at 5.0 ms, an afterpeak increase in emission ensues. In the presence of 1% nitrogen, this effect is almost completely absent. To answer an earlier question, these experiments show that the added nitrogen does *prevent* the metastable atoms from forming in the afterpeak, possibly in addition to quenching any that do form. There are two possible methods for  $N_2$  intervention in the CRC process: (1) the nitrogen reduces the capacity for argon ions to participate in recombination; and (2) the nitrogen reduces the capacity for electrons to participate in recombination.

### 3.3.1. Effect of $N_2$ on argon ions

To test the validity of the first possibility given above, the argon ion signal was observed via ToF-MS at different times during the pulse cycle. Fig. 8 shows that in the steady-state plasma (observed between 4 and 5 ms), the addition of 1% nitrogen

reduced the argon ion signal by a factor of  $\sim 10$ . Wagatsuma and Hirokawa [65] observed a similar reduction in argon ions. The reduction in argon ions here is thought to arise from charge transfer reactions with the nitrogen molecules [66,67]



followed by dissociative recombination of the nitrogen molecular ion with an electron.



Reaction (2) has a rate constant of  $\sim 5 \times 10^{-11} \text{ cm}^3 \text{ s}^{-1}$  (although the exact rate is somewhat pressure and electron-density dependent) [66,67]. Given a number density of  $N_2$  of  $\sim 3 \times 10^{14} \text{ cm}^{-3}$  ( $8 \times 10^{-3}$  torr) the quenching rate should be in the order of  $\sim 10^4 \text{ s}^{-1}$ . Indeed, using the  $\text{Ar}^+$  signals in the lower plot of Fig. 8 to create a plot of  $\log(\text{ion signal})$  vs. time after pulse termination, the slope reveals the loss rate of  $\text{Ar}^+$  with 1%  $N_2$  present to be  $\sim 10^5 \text{ s}^{-1}$ , in excellent agreement with the predicted rate. This implies that the added nitrogen offers a very fast method for plasma recombination to occur and, in the process, prevents argon ions from forming the highly excited neutral states normally observed in the afterpeak.

### 3.3.2. Effect of $N_2$ on electrons

The addition of 1% nitrogen to the plasma shows a reduction in the number density of argon ions and a reduction in the capacity for argon ion–electron recombination in the afterpeak. By varying the concentration of nitrogen, it is also possible to determine an electron-energy effect. Fig. 9 shows the emission at 811.5 nm as a function of time at different partial pressures of nitrogen. The method for adjusting the partial pressures was to close the nitrogen valve and allow the vacuum pump to slowly remove the nitrogen. Before closing the valve, the plasma established the usual operating condition of  $\sim 1$  mtorr ( $\sim 1\%$  by vol.) of  $N_2$  in the 0.8-torr Ar plasma. While this experiment does not provide quantitative results, the observations that it does provide are informative.

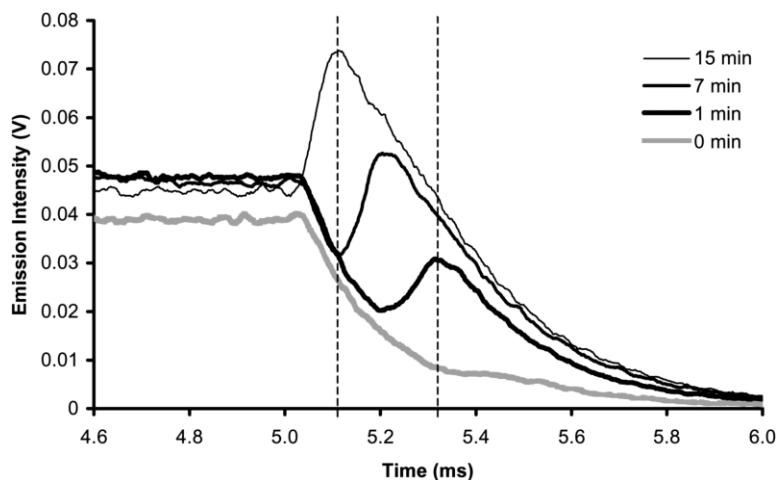


Fig. 9. Emission from the 811.5-nm line as a function of time to show the effect of decreasing nitrogen in the discharge. The times labeled in the figure refer to the time after the nitrogen valve was closed. Measurements made 5 mm above the cathode, 5.0-ms pulse length, 25% duty cycle, 0.8-torr Ar,  $\sim 1.5$ -W peak power, Fe cathode.

As nitrogen is pumped out of the discharge region, an afterpeak appears within the first minute. The peak is small and has a peak maximum later than 5.3 ms. As more nitrogen is removed from the plasma, the afterpeak increases in intensity and appears closer in time to the termination of discharge power. After 15 min, the plasma resembles 'pure' conditions and the afterpeak maximum is close to 5.1 ms.

Increasing the partial pressure of nitrogen has the unquestionable effect of delaying the appearance of the afterpeak, and in so doing, reduces the intensity of the emissions when they finally do appear. The number densities of argon ions was not determined in a comparative experiment, but we will assume that the steady-state values of  $[\text{Ar}^+]$  will vary somewhat linearly with the nitrogen concentration between the two limits established in Fig. 8. Charge transfer reactions between argon ions and nitrogen molecules could feasibly account for the difference in emission intensity in the afterpeak, because increasing  $[\text{N}_2]$  would decrease the number of argon ions available for recombination. Although this mechanism can account for the intensity of the afterpeak emissions, it does not explain the delayed appearance at higher concentrations of  $\text{N}_2$ .

Because recombination is inefficient until electrons reduce their kinetic energy to the gas temperature, a time delay between voltage termination and recombination will be observed while the electrons collisionally cool with bath gas atoms [68,69]. Although the addition of lighter, atomic ions can speed up this thermalization process [70], vibrationally excited molecular species can slow down the process [52,71,72]. The latter effect is caused by superelastic collisions between electrons and (mostly) vibrationally excited molecules; the vibrational temperature of the nitrogen can be an order of magnitude larger than the rotational temperature under similar operating conditions [23,24,71].

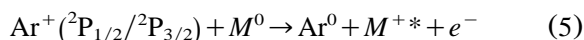
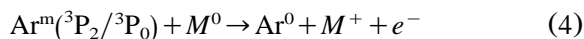
The time required for nitrogen to attain these high vibrational states is in the order of  $10^{-5}$  to  $10^{-3}$  s [71,72] so the electron-temperature decrease in the afterpeak will be highly dependent on the pulse width—operating the PGD in the microsecond regime may not display the superelastic-collision effect. The internal energy contained in the various modes of the nitrogen molecule can increase the time the electrons take to reach the low temperatures required for efficient recombination. At high nitrogen concentrations (time zero in Fig. 9), superelastic collisions almost

completely prevent the electrons from thermalizing before they are lost by ambipolar diffusion [2] to the chamber walls. Under these conditions, recombination effects are not observed. As the quantity of nitrogen decreases—with increasing time after the valve closure—the possibility for superelastic collisions decreases, so the time-delay before recombination occurs also decreases.

The effects of 1% nitrogen on afterpeak processes are shown to be multifaceted. At 1% nitrogen, charge transfer with argon ions—and subsequent dissociative recombination of the resultant nitrogen ions—decreases the number density of argon ions by an order of magnitude. High-energy vibrational modes, developed during the 5 ms before the voltage termination, prevent electrons from kinetically cooling in the afterpeak. Consequently, very little recombination occurs for argon ions and the afterpeak emissions are vastly reduced. As the nitrogen concentration decreases, fewer argon ions are removed by charge transfer reactions, fewer superelastic collisions are possible for electrons, and more CRC occurs for argon in the afterpeak.

### 3.4. Effect of $N_2$ on analyte signals

Whereas the excitation of sputtered analyte atoms in GDs and PGDs occurs almost exclusively by electron excitation, ionization occurs by three predominant processes [2,5,6,8]. These processes are Penning ionization (PI) [73], charge transfer (CT), and electron ionization, given, respectively, by the three equations below.



$\text{Ar}^m$  refers to one of the metastable states of argon (at 11.55 and 11.72 eV),  $M^0$  is the ground state sputtered metal atom, and  $\text{Ar}^0$  is the ground state of argon, and  $M^{+*}$  is a ground- or excited ion state of the metal. If the ionization potential (IP)

of  $M$  is less than the metastable state of argon (as is the case for all metals in the periodic table), then PI will occur at approximately one-fifth of the collision frequency [44,74]. If the second IP of  $M$  is also below the metastable states, as is common for the rare earth elements [75],  $M$  can be doubly-ionized in a single PI collision [76,77]. Several reports have shown that Penning ionization is one of the most dominant ionization mechanisms in unconfined GDs below 2 torr [30,78]. When operated at higher pressures, such as in the Grimm source [18,22,49,79–86], or when confined, such as in hollow cathode geometries [82,86–89], excitation and ionization are less dependent on metastable atom populations. At higher pressures, metastable atom number densities are reduced by increases in metastable–metastable collisions, electron de-excitation, and collisional de-excitation by atoms and ions. The optimum pressure range for maximum metastable atom formation is  $\sim 0.8$  torr [58,90,91], as used in these studies.

CT reactions are most efficient when an efficient overlap exists between the argon ion and the neutral with which it reacts [92]. The  $^2\text{P}_{1/2}$  ground state argon ion overlaps well with an excited state of the copper ion, resulting in enhanced population of this state with respect to states close in energy. This enhancement of the 224.7-nm line for Cu II, indicating CT, has been witnessed mostly in higher pressure ( $> 1$  torr) discharges [17,20,82,83,93], and less so in lower pressure GDs [91].

Electron excitation and ionization are more dominant in higher-pressure GDs when PI contributions are reduced. Electron temperatures and excitation temperatures have been determined in a number of different steady-state glow discharge sources using a number of different methods. Langmuir probe measurements [78] and spectroscopic studies [23,24,45,79,94–96] show that the electron temperature is not particularly sensitive to operating conditions, but is sensitive to the sample cathode [78].

Of these three mechanisms, Penning ionization is expected to dominate ionization processes, while electron excitation from the ground state is expected to dominate the excitation processes for the sputtered atoms. Charge transfer, while possible

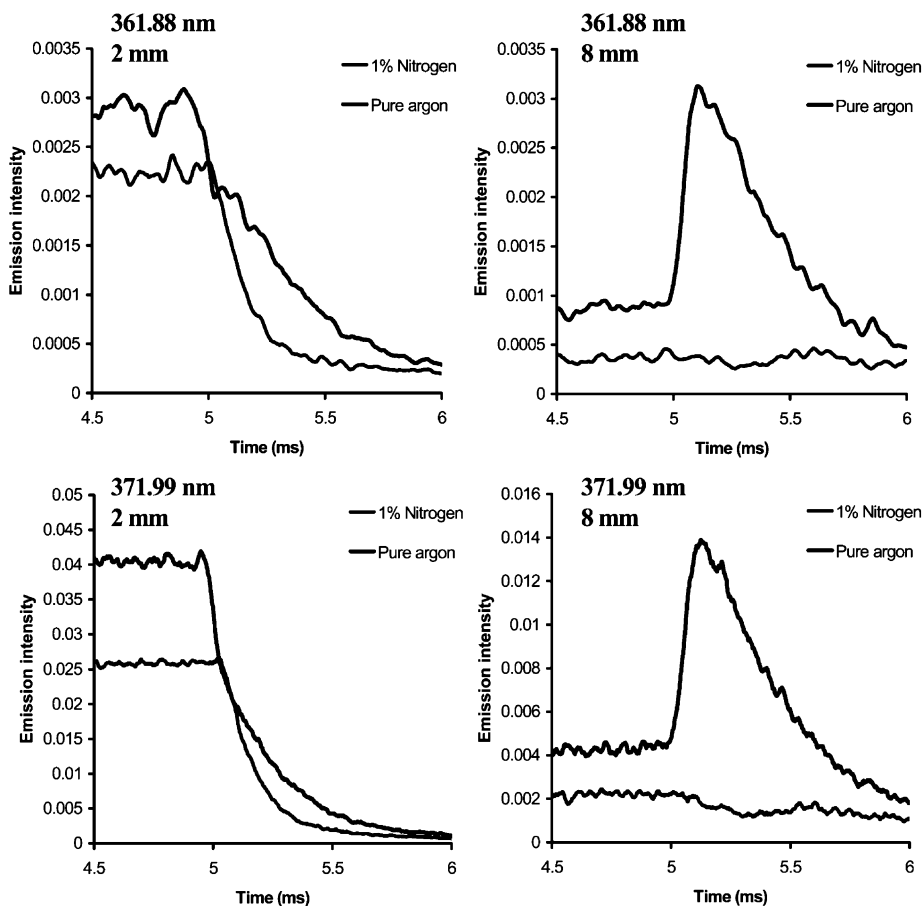


Fig. 10. Effect of 1% nitrogen on sputtered iron atom emissions. Each plot is labeled according to the emission wavelength and sampling height above the cathode. Pulse length: 5.0 ms, 25% duty cycle, 0.8-torr Ar,  $\sim 1.5$ -W peak power, Fe cathode.

for iron [97], is not expected to be so important at these pressures.

#### 3.4.1. Fe atomic emission

Fig. 10 shows the effect of 1% nitrogen addition on the emission signals of Fe I. The two lines observed are the  $3d^64s4p-3d^64s^2$  (3.33–0.00 eV) transition at 371.99 nm, and the  $3d^74p-3d^74s$  (4.41–0.99 eV) transition at 361.88 nm. The heavy lines are the emissions collected under normal operating conditions (no nitrogen added) and behave similarly to the copper lines discussed elsewhere [98,99]. Close to the cathode ( $< 2$  mm), very little afterpeak is observed, and further from the cathode ( $> 3$  mm) the afterpeak intensity

increases, relative to the steady-state signals. The CRC process that occurs when the voltage is removed accounts for the presence of the afterpeak. Fig. 10 shows that when 1% nitrogen is added the afterpeak emissions are no longer prevalent. This follows the same trend observed for argon atom emissions described above. With 1% nitrogen added, high-lying vibrational states—excited during voltage-on period—provide kinetic energy to electrons in the afterpeak via superelastic collisions. The electrons, therefore, take longer to thermalize and consequently some will be lost by diffusion to the walls; thus the CRC is reduced.

The reduction in emission intensity during the steady state could be caused by a reduction in

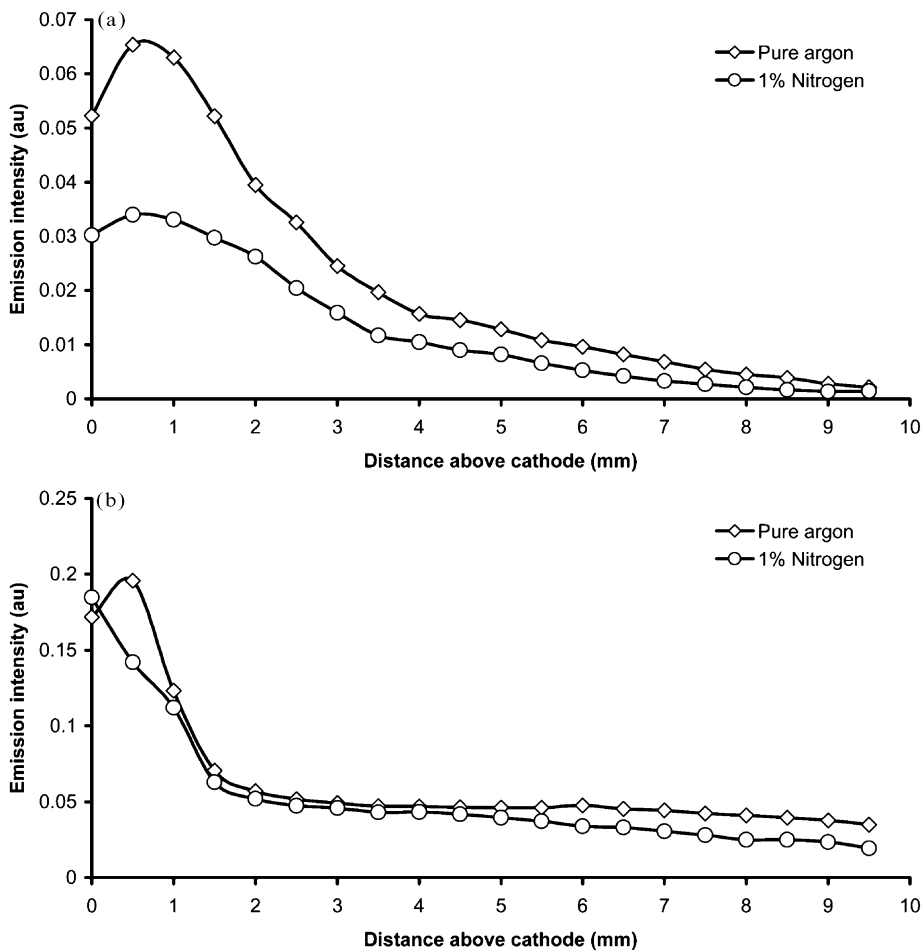


Fig. 11. Emission intensity at 4.9 ms at (a) 371.99 nm and (b) 811.5 nm as a function of distance above the cathode. Conditions given in Fig. 10.

electron temperature or number density. The nitrogen absorbs energy into internal modes during the voltage-on period [52,72], and this energy transfer process presumably reduces the electrons' kinetic energy. In the absence of electron-temperature measurements, such speculation cannot be validated. Wagatsuma and co-workers have shown that reduced emission intensities in Ar/N<sub>2</sub> plasmas could be caused, in part, by a reduction in sputtering rate [17]. A lower sputtering rate, and hence lower atom number density in the plasma would cause a uniform reduction in emission intensity. Fig. 10 shows that the reduction in emission intensity in the steady-state is indeed fairly uniform

in space with approximately 50% reduction. This is shown more clearly in Fig. 11a, where the steady-state emission at 371.99 nm is plotted as a function of distance. The same effect is not as conspicuous for the bulk plasma gas (argon) as seen by the emission intensity at 811.5 nm in Fig. 11b. The emissions are not reduced to the same extent as the iron lines, indicating the specificity of emission reduction.

Fang and Marcus report that reduced sputter yields are expected when lighter atoms are used as projectiles for cathodic sputtering [78]. The occurrence of N<sub>2</sub><sup>+</sup> or N<sup>+</sup> charge carriers impinging on the cathode surface could produce the lower

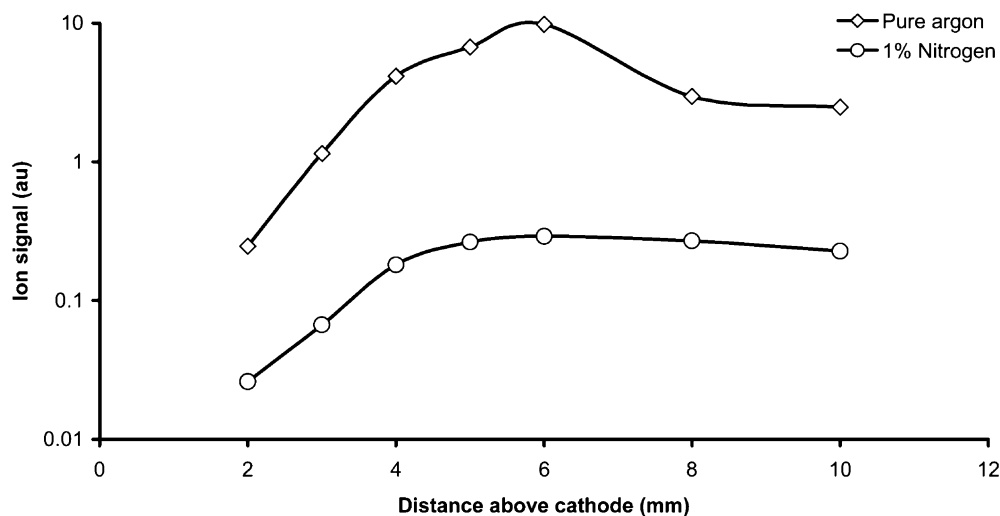


Fig. 12.  $^{56}\text{Fe}^+$  ion signals as a function of sampling height above the cathode to show the effect of 1% nitrogen on the ionization of sputtered metal atoms. Ion signals measured at 4.9 ms, representing steady-state conditions. Pulse length: 5.0 ms, 25% duty cycle, 0.8-torr Ar,  $\sim 1.5$ -W peak power, Fe cathode.

sputtering yields. Wagatsuma and Hirokawa note with the introduction of relatively small amounts of nitrogen into argon GDs (<1%), the emission intensity is a good predictor of the sputtering rate (as determined gravimetrically) [18]. The 40–50% reduction in emission intensity observed here indicates a 40–50% decrease in sputter rate.

#### 3.4.2. Fe ion signals

Fig. 12 shows the  $^{56}\text{Fe}^+$  signal as a function of sampling distance above the cathode taken at 4.9 ms after pulse initiation. These signals exemplify steady-state signals. The addition of 1% nitrogen drastically reduces the iron signals but the effect is not uniform across the discharge (notice the logarithmic scale). Close to the cathode (2–4 mm), iron ion signals are reduced by factors of 10–20, but at greater sampling distances (5–7 mm), iron ion signals decreased by up to a factor of 30. The difference between emission attenuation factor (2 throughout) and ion attenuation factor (10–30) for Fe is too great to be due to an experimental artifact. Clearly, excitation and ionization processes are strongly decoupled, especially in the region above 4 mm.

This decoupling was also observed by Ratliff and Harrison [16] by the time-dependent emission

and ion signal monitoring of Cu in response to pulses of water vapor introduced into the GD. Cu emissions were only briefly reduced by the introduction of a pulse of  $\text{H}_2\text{O}$ , but Cu ion signals were reduced for a considerably longer time. This indicates that although the electron energy distribution function (EEDF) was only slightly affected by the pulse of  $\text{H}_2\text{O}$ , the mechanism responsible for ionizing the copper was more sensitive to the trace amounts of water. This decoupling demonstrates the minor role that electrons play in ionizing sputtered atoms under these conditions, and the major role that the metastable argon atoms play via Penning ionization.

#### 3.5. Effect of nitrogen on other ion intensities during voltage-on period

The addition of 1% nitrogen to the plasma had different effects on different ions in the spectra. All the sputtered analyte ion signals responded in a similar way, with attenuation factors in the range 5–30 (depending on distance) as demonstrated for  $^{56}\text{Fe}^+$  and  $^{52}\text{Cr}^+$  in Fig. 13. The addition of nitrogen also reduced the number of  $\text{Ar}^+$  ions by factors of 5–13 (as expected by charge transfer collisions) and  $\text{Ar}_2^+$  ions by factors of 2–13,

depending on distance, with the largest attenuation occurring at  $\sim 4\text{--}6$  mm. The  $\text{ArH}^+$ ,  $\text{H}_3^+$  and  $\text{Ar}^{2+}$  signals were considerably more attenuated by the addition of nitrogen than all the other ions in the spectra.

The added nitrogen completely eliminated the  $\text{H}_3^+$  signal.  $\text{ArH}^+$  and  $\text{Ar}^{2+}$  signals were reduced by factors of 10–100, as shown in Fig. 14. These ions are obviously much more sensitive to the  $\text{N}_2$  addition than  $\text{Ar}^+$ ,  $\text{Ar}_2^+$ , or the other ions. This behavior would be consistent if the three ions in question required two excited or ionized argon atoms as precursors, and all the other attenuated ions only relied on one excited/ionized precursor. Under these circumstances, a decrease in the excited/ion states of argon would decrease the  $\text{H}_3^+$ ,  $\text{ArH}^+$  and  $\text{Ar}^{2+}$  ions to the square of the loss of the excited/ion states, but would reduce the other ions proportionally to the loss of excited/ion states.

The most probable population mechanism for populating the 27.63-eV ground state of  $\text{Ar}^{2+}$  is electron excitation.



The vast reduction in the  $\text{Ar}^{2+}$  ions would require that the high-energy tail of the EEDF be drastically

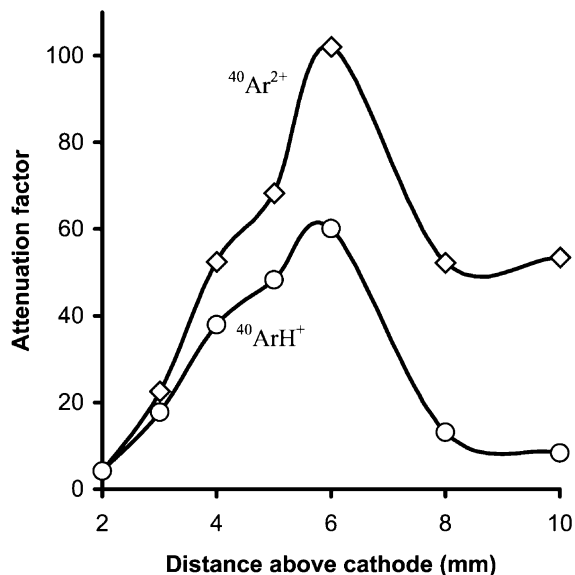


Fig. 14. Attenuation factors for the steady-state signals of  $\text{Ar}^{2+}$  and  $\text{ArH}^+$  in response to the addition of 1% nitrogen. Conditions given in Fig. 10.

reduced by the addition of 1% nitrogen. Indeed, the ability for nitrogen to undergo inelastic collisions with electrons and to absorb the electron's kinetic energy is well known [100–102]. Even at concentrations as low as 1% in argon, nitrogen

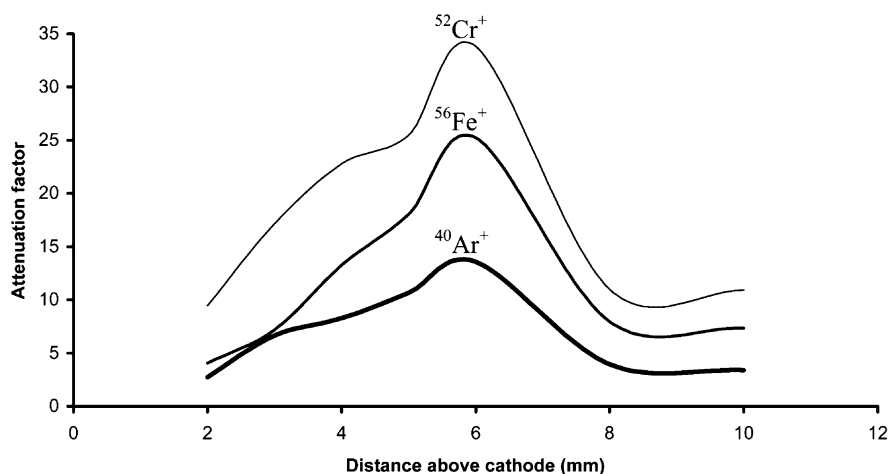
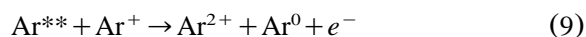


Fig. 13. Attenuation factors for the steady-state signals of different ions vs. distance above the cathode in response to the addition of 1% nitrogen. Conditions given in Fig. 10.

greatly reduces the average energy of the EEDF. Two other energetically feasible reactions for the formation of doubly charged argon ions are given by the equations,

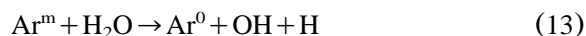


where  $\text{Ar}^{**}$  is an excited state of argon above 13.81 eV (8) or 11.9 eV (9), respectively. No reference to these reactions could be found in the literature. Reactions (8) and (9) both rely on two highly energetic states of argon to produce the doubly charged ion, and would consequently be sensitive to the square of a reduction in  $\text{Ar}^{**}/\text{Ar}^+$ , as required.

Possible reactions leading to the formation of  $\text{ArH}^+$  are [12,103,104]



In order to be thermo-neutral, reactions (10) and (11) require total internal energies of 13.1 and 13.5 eV, respectively (neglecting kinetic energy effects) [75,105]. This would require an energy level above the 4s metastable states of argon. Reaction (12) can proceed if the excited state is one of the metastable states at 11.55 or 11.72 eV. The formation of H in reaction (12) can occur by a variety of reactions, including [103]

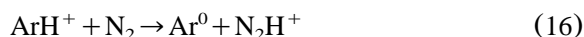


both of which are exothermic as written and require a highly-energetic precursor.

The dominant formation mechanism for  $\text{H}_3^+$  is expected to be [103]

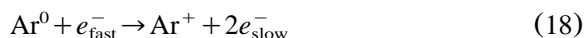


which is exothermic as written. In this case, the formation of  $\text{H}_3^+$  is therefore dependent on the  $\text{ArH}^+$  precursor. The vast reduction in  $\text{ArH}^+$  by the addition of 1% nitrogen is presumably the cause for the elimination of  $\text{H}_3^+$ . The added nitrogen is also able to prevent/decrease the formation of  $\text{H}_3^+$  by the reactions



that are presumably exothermic based on the appearance of large quantities of  $\text{N}_2\text{H}^+$  in the spectra with nitrogen added. Reaction (16) should proceed at a rate similar to that for the CT reaction between  $\text{Ar}^+$  and  $\text{Fe}^0$ , so the additional destruction channel for  $\text{ArH}^+$  can only account for a  $\sim 5$ – $13$ -fold reduction in signal. Again, this suggests that nitrogen is preventing the formation of  $\text{ArH}^+$ , as well as providing additional destruction channels.

The argon ions can be formed directly by electron ionization, or be electron ionization from the metastable states.



The reduction of argon ions observed in Fig. 13 might be related to additional destruction mechanisms created by the added nitrogen, rather than inhibiting a production process. One such additional loss process induced by  $\text{N}_2$  is the charge transfer reaction given in reaction (2). The reduction in the metal ion signals in the steady-state regime is undoubtedly related to the reductions in sputter yield and metastable states. The fact that the sputtering rate decreased by a factor of  $\sim 2$ , but the ionization efficiency decreased by a factor of 5–30, is testimony to the importance of PI in ionizing the sputtered atoms.

It is also possible that that the added nitrogen introduces additional destruction mechanisms for

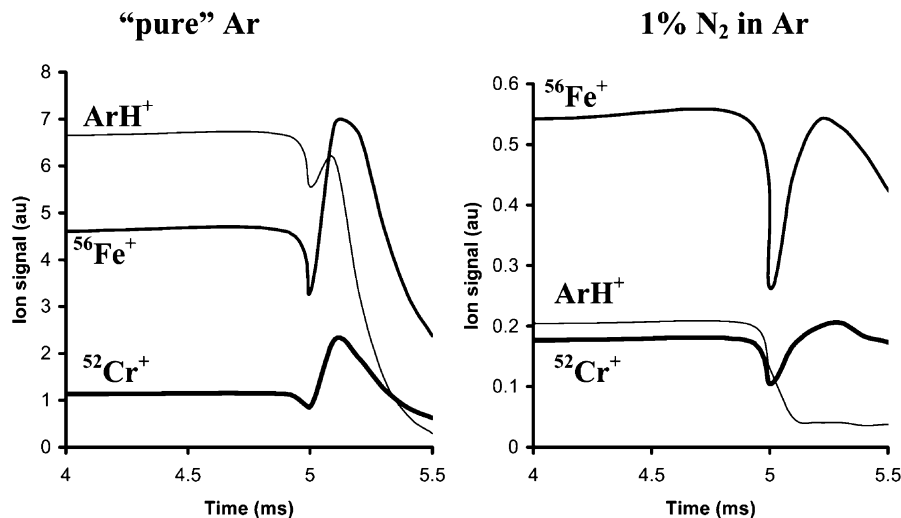


Fig. 15. Selected ion signals as a function of time to show the effect of added nitrogen. Sampling height: 5 mm, 5.0-ms pulse length, 25% duty cycle, 0.8-torr Ar, ~1.5-W peak power, Fe cathode.

ArH<sup>+</sup>, H<sub>3</sub><sup>+</sup> and Ar<sup>2+</sup>. If CT between Ar<sup>2+</sup> and N<sub>2</sub> is a quantum-allowed process and occurred at the collision frequency, the rate for this reaction would be approximately twice as fast as the CT reaction between Ar<sup>+</sup> and N<sub>2</sub> [106]. Based on this premise, the added nitrogen would reduce Ar<sup>2+</sup> signal by factors of 10–26, depending on height above the cathode. That the attenuation factor is twice this large again indicates that the nitrogen must also be reducing the formation of Ar<sup>2+</sup>.

The preceding discussion shows that there are several mechanisms to explain the extreme attenuation rates of H<sub>3</sub><sup>+</sup>, ArH<sup>+</sup>, and Ar<sup>2+</sup> compared to the other ion signals. The formation of these ions requires either very high-energy electrons (>27 eV), or at least two highly excited or ionized states of argon as precursors. Nitrogen is known to reduce the kinetic energy of electrons when added at 1% to argon plasmas, and is shown to reduce both the metastable states and the ion states of argon. The other ions are less affected by the addition of N<sub>2</sub> (metal ions, Ar<sup>+</sup> and Ar<sub>2</sub><sup>+</sup>) because they rely on lower energy electrons and/or one excited state of argon. Consideration of additional loss channels created by the addition of nitrogen will contribute to the reduction in the discussed

ion signals, but alone cannot account for the attenuation factors observed.

### 3.6. Effect of nitrogen on the ion intensities in the afterpeak time regime

The added nitrogen is shown to have a large effect on ion signals in the 4–5-ms time regime. At this time, the plasma is essentially in the steady state. Optical experiments show that when the voltage is terminated at the end of the 5-ms pulse, analyte ions (and argon ions) recombine. One might assume that the observed emissions from the sputtered metal atoms would signify a decrease in the analyte ions in the afterpeak period. That this is not the case has been demonstrated on numerous occasions [38–41,43]. Fig. 15 shows a typical response for various ions under normal operating conditions. The argon ion signal is not shown here because its temporal characteristics have already been discussed in detail (see discussion on Fig. 8). With no nitrogen added, the Fe<sup>+</sup> and Cr<sup>+</sup> ion signals decrease immediately following pulse termination, but quickly increase to a maximum at approximately 5.1 ms. The afterpeak maximum is noticeably larger than the steady-state

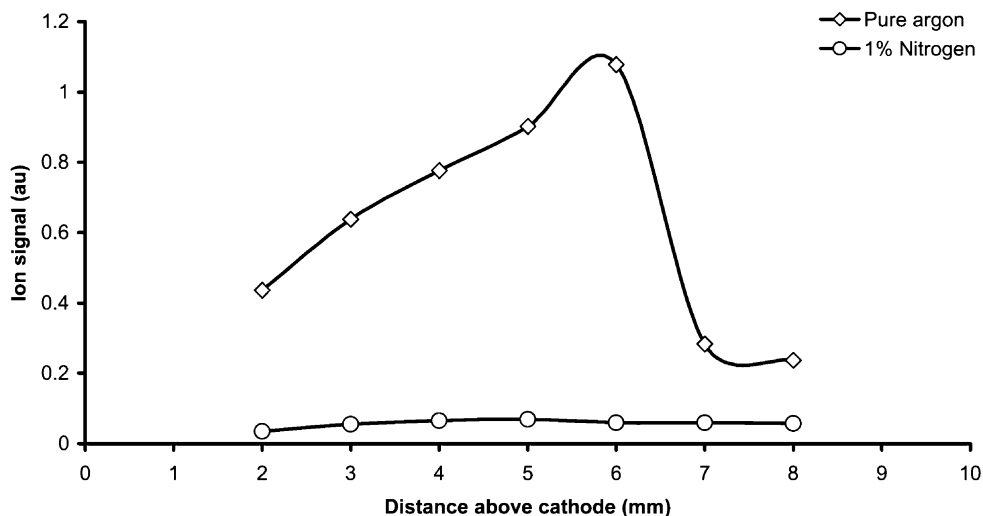


Fig. 16.  $^{56}\text{Fe}^+$  signal, determined by ToF-MS, as a function of distance to show the effect of 1% nitrogen on ionization in the afterpeak. Pulse length: 5.0 ms, 25% duty cycle, 0.8-torr Ar,  $\sim 1.5\text{-W}$  peak power, Fe cathode.

signal. After 5.1 ms the ion signals decay in a reasonably exponential manner.  $\text{ArH}^+$  displays similar behavior, but the afterpeak maximum is smaller with respect to the steady-state value, and the decay rate is considerably faster. It is assumed that the faster decay rate is due to the faster recombination rate of the diatomic  $\text{ArH}^+$ , as opposed to the monatomic  $\text{Fe}^+$  and  $\text{Cr}^+$ .

With 1% nitrogen added, the  $\text{ArH}^+$  ion is severely quenched (as discussed above) and no evidence for afterpeak formation is observed. If the  $\text{ArH}^+$  in the afterpeak were formed from  $\text{Ar}^+$  precursors, the afterpeak signal for  $\text{ArH}^+$  should scale with the steady-state signal of  $\text{Ar}^+$ . That this is not the case, coupled with the fact that the  $\text{ArH}^+$  is severely quenched in the afterpeak is further evidence for neutral precursors to the formation of  $\text{ArH}^+$ , reactions (10)–(12) above.

After the addition of nitrogen, the afterpeaks are more delayed for  $\text{Fe}^+$  and  $\text{Cr}^+$ , maximizing at  $\sim 5.3$  ms, and are of approximately the same magnitude as the steady-state signals. The afterpeak ion signals are smaller than in pure argon, and are more delayed in time. These findings are entirely consistent with the emission experiments discussed earlier, namely, with added nitrogen, afterpeak emission intensities are reduced in inten-

sity and delayed in time. Although somewhat counter-intuitive, these results demonstrate, unequivocally, that ionization and recombination of the sputtered metal atoms and ions are both enhanced in the afterpeak. These observations are rationalized if the recombination effects follow the ionization effects in time.

Metastable argon atoms, formed during the afterpeak, Penning ionize the sputtered metal atoms and increase the number of these metal ions. The sputtered metal ions then participate into CRC, occupying the highest energy levels most abundantly, and decaying radiatively to the ground state. The addition of nitrogen delays the thermalization of the electrons, which in turn delays the recombination of argon ions with electrons. This delays the appearance of metastable states, which delays the appearance of the Penning ionized metal ions.

Consistent with this model are some additional interesting observations. Figs. 16–18 show the effect of 1% nitrogen on the afterpeak signals of, respectively, the iron ion (determined by ToF-MS), iron recombination (determined by AE), and iron ion signals (determined by AA). In the pure argon discharge, afterpeak ion signals determined by MS and AA and afterpeak emission signals maximize

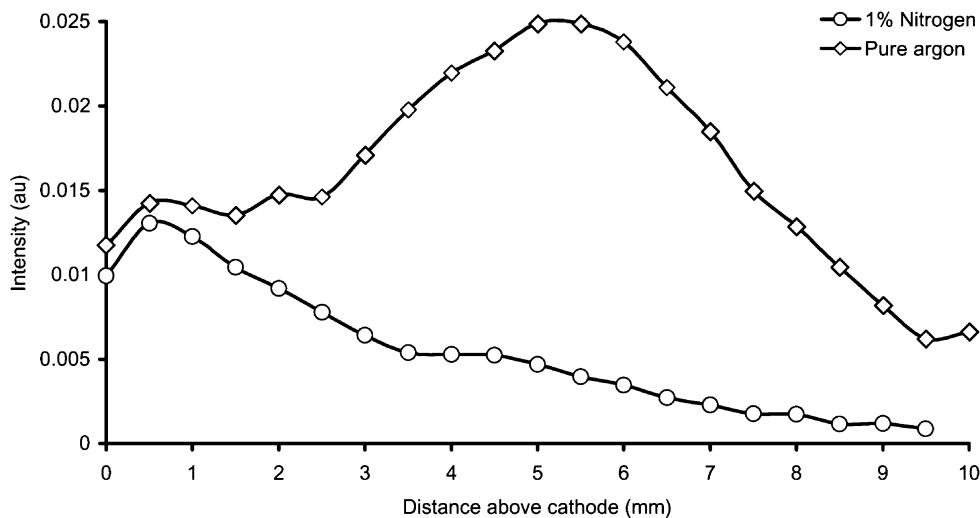


Fig. 17. Emission intensity at 371.99 nm for the Fe I line as a function of distance to show the effect of 1% nitrogen on the afterpeak. Conditions given above.

at approximately 5–6 mm above the cathode. Afterpeak signals in all cases display a steady, but small, decrease closer than 6 mm and larger decreases at distances greater than 6 mm. The addition of nitrogen prevents PI reactions from occurring and this diminishes the metal ion for-

mation in the afterpeak, as observed by AA and ToF-MS. The ions are not available for recombination, so emissions from excited atom states are also diminished.

Because of the prolonged production of metal ions by PI compared to argon ions, one might also

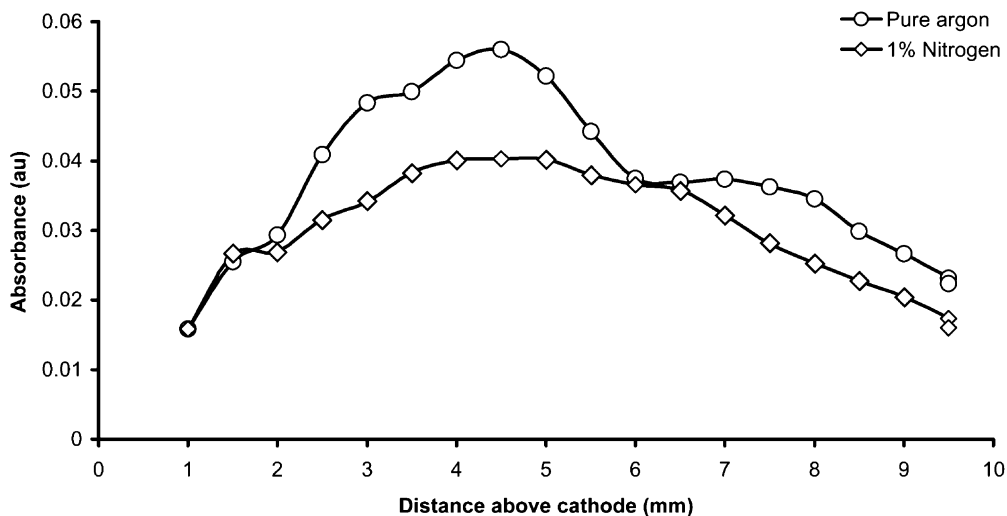


Fig. 18. Iron ion absorbance at 259.9 nm as a function of distance above the cathode to show the effect of 1% nitrogen addition on the afterpeak. Absorption measurements taken at 5.5 ms.

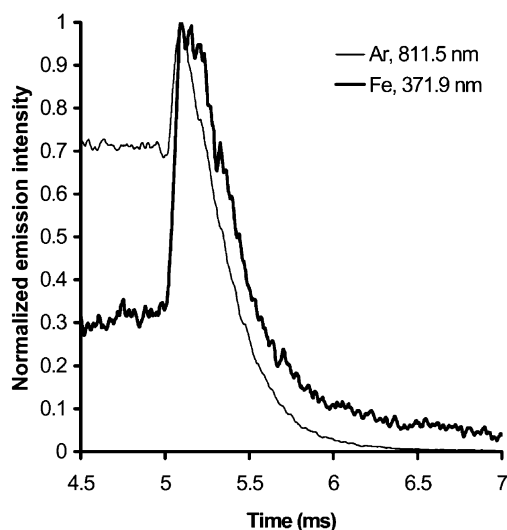


Fig. 19. Comparison of the afterpeak emissions for Ar I and Fe I with no nitrogen added. Data collected at 4 mm above the cathode, 5.0-ms pulse length, 25% duty cycle, 0.8-torr Ar,  $\sim 1.5$ -W peak power, Fe cathode.

anticipate that the iron emissions should also be prolonged. The data illustrated in Fig. 19 show that this is indeed the case. The afterpeak for the Fe atom emission at 361.88 nm appears slightly later than the Ar atom emission at 811.5 nm, and maintains this maximum longer than the argon atom emission. While the decay rates are very similar after the afterpeak maximum, the Fe emissions do not reach a base-line level, as do the argon atom emissions. This behavior is not unique to these transitions, but is found for all Ar atom and Fe atom lines studied in this laboratory. Assuming that the two- or three-body recombination rates are not significantly different for  $\text{Ar}^+$  and  $\text{Fe}^+$ , the prolonged emissions for the Fe atoms must be due to the continual formation of Fe ions by PI.

Using a power supply with a slower fall-time, similar results were also observed with a copper cathode. Fig. 20 shows that the emission from the copper atom lines is considerably more prolonged than the emission from the argon atom lines, indicating that the mechanisms discussed above are not unique to iron (indeed, chromium present in the iron cathode also showed similar AE and

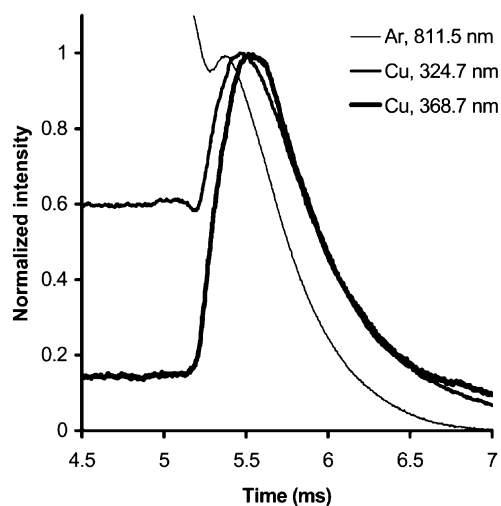


Fig. 20. Comparison of the afterpeak emissions for Ar I and Cu I with no nitrogen added. Data collected at 4 mm above the cathode, 5.0-ms pulse length, 25% duty cycle, 0.8-torr Ar,  $\sim 1.5$ -W peak power, Cu cathode. The power supply used here has a slower fall-time than in Fig. 19.

MS behavior to iron). The delayed responses of the Ar I and Cu I emissions, when the slower fall-time power supply was used, is also consistent with the proposed mechanism in the afterpeak. The slower fall time prevents the electrons from cooling as quickly and delays the onset of recombination. Notice, again, how the tailing on the Cu I emissions does not decay to zero, but is more prolonged than the Ar I emission. This asserts that the highly excited states of copper are continuing to emit long after electron excitation is a possible excitation mechanism, implying that PI followed by recombination is the most probable mechanism.

#### 4. Conclusions

The addition of  $\sim 1\%$  of nitrogen to a 0.8-torr plasma has provided insight into the mechanisms of excitation and ionization in the PGD. Optical absorbance and emission measurements demonstrate the transfer of energy from excited argon atoms to nitrogen molecules during the voltage-on period, with a subsequent reduction in the number of metastable states of argon. This reduction in metastable atoms reduces the ionization of sput-

tered atoms during the voltage-on period, but does not significantly impact emissions from excited analyte atoms because the latter are created mostly via collisions with electrons.

Attenuation factors for  $\text{ArH}^+$  and  $\text{Ar}^{2+}$ , are more than twice as great as for  $\text{Ar}^+$ , indicating that these ions are either reliant upon two highly energetic precursors (both of which are attenuated by the added nitrogen), or are reliant on one energetic precursor and have an additional destruction pathway with nitrogen. Further study is required to determine the exact mechanisms in these conditions.

When the voltage is terminated in the 'pure' argon discharge, ToF-MS data and optical experiments show that argon ion recombination leads to an increase in metastable states. This, in-turn, leads to an increase in the propensity for Penning ionization. Metal ions and emissions (from recombining metal ions) are observed for several milliseconds after pulse termination. When nitrogen is added it prevents electrons from collisionally cooling in the afterpeak due to superelastic collisions with vibrationally excited states of  $\text{N}_2$ , formed during the voltage-on period. These superelastic collisions delay the onset of recombination because fast electrons recombine less-readily than slow electrons. During this delayed electron-cooling period, ions and electrons are lost by diffusion to the walls with the result that fewer recombination reactions occur when the conditions are eventually permissible. The afterpeak delay, and magnitude, is shown to be controllable by the nitrogen partial pressure. The reduction in afterpeak emissions caused by the addition of nitrogen could provide a lower background environment for AAS and AFS experiments, while allowing the AAS and AFS measurements to be made closer in time to the voltage-off period. This would allow measurements to be made at a time of maximum sputtered atom density—as they will not have had time to diffuse away. Also, the ability for nitrogen to quickly remove argon ions and delay the onset for the production of sputtered analyte ions could be particularly useful for reducing the interference of discharge-gas species in time-gated MS measurements [37,38]. While nitrogen was intended to be used only as a diagnostic tool in these experi-

ments, it turns out that controlled additions of nitrogen to PGDs might actually be highly beneficial for time-gated AAS, AFS [and laser-induced atomic fluorescence (LIAF)] and MS analytical methods.

## References

- [1] C.M. Barshick, Glow discharge mass spectrometry, in: C.M. Barshick, D.C. Duckworth, D.H. Smith (Eds.), *Inorganic Mass Spectrometry*, Marcel Dekker, Inc, New York, 2000.
- [2] B. Chapman, *Glow Discharge Processes*, ed, John Wiley and Sons, New York, 1980.
- [3] D.C. Duckworth, C.M. Barshick, Ion traps: what do they hold for elemental analysis?, *Anal. Chem.* 70 (1998) 709A–717A.
- [4] D.C. Duckworth, R.K. Marcus, Sampling an rf-powered glow discharge source with a double quadrupole mass spectrometer, *Appl. Spectrosc.* 44 (1990) 649–655.
- [5] W.W. Harrison, K.R. Hess, R.K. Markus, F.L. King, Glow discharge mass spectrometry, *Anal. Chem.* 58 (1986) 341A–356A.
- [6] F.L. King, W.W. Harrison, Glow discharge mass spectrometry: an introduction to the technique and its utility, *Mass Spectrosc. Rev.* 9 (1990) 285–313.
- [7] F.L. King, J. Teng, R.E. Steiner, Glow discharge mass spectrometry: trace element determination in solid samples, *J. Mass Spectrosc.* 30 (1995) 1061–1075.
- [8] R.K. Marcus, *Glow Discharge Spectroscopies*, 1st ed, Plenum Press, 1993.
- [9] D. Stuewer, Glow discharge mass spectrometry—A versatile tool for elemental analysis, *Fresenius' J. Anal. Chem.* 337 (1990) 737–742.
- [10] J.W. Coburn, A system for determining the mass and energy of particles incident on a substrate in a planar diode sputtering system, *Rev. Sci. Instr.* 41 (1970) 1219–1223.
- [11] S. De Gendt, R.E. Van Grieken, S.K. Ohorodnik, W.W. Harrison, Parameter based evaluation for the analysis of oxide-based samples with radio frequency glow discharge mass spectrometry, *Anal. Chem.* 67 (1995) 1026–1033.
- [12] P.F. Knewstubb, A.W. Tickner, Mass spectrometry of ions in glow discharges. II. Negative glow in rare gases, *J. Chem. Phys.* 36 (1962) 684–693.
- [13] T.J. Loving, W.W. Harrison, Dual-pin cathode geometry for glow discharge mass spectrometry, *Anal. Chem.* 55 (1983) 1526–1530.
- [14] S.K. Ohorodnik, W.W. Harrison, Cryogenic coil for glow discharge sources, *Anal. Chem.* 65 (1993) 2542–2544.
- [15] P.H. Ratliff, W.W. Harrison, The effects of water vapor in glow discharge mass spectrometry, *Spectrochim. Acta Part B* 49 (1994) 1747–1757.

- [16] P.H. Ratliff, W.W. Harrison, Time-resolved studies of the effects of water vapor in glow discharge mass spectrometry, *Appl. Spectrosc.* 49 (1995) 863–871.
- [17] K. Wagatsuma, Emission characteristics of mixed gas plasmas in low-pressure glow discharges, *Spectrochim. Acta Part B* 56 (2001) 465–486.
- [18] K. Wagatsuma, K. Hirokawa, Characterization of atomic emission lines from argon, neon and nitrogen glow discharge plasmas, *Anal. Chem.* 57 (1985) 2901–2907.
- [19] K. Wagatsuma, K. Hirokawa, Quenching mechanisms in argon–nitrogen or neon–nitrogen glow discharge plasmas, *Anal. Chem.* 61 (1989) 326–329.
- [20] K. Wagatsuma, U. Danzaki, Non-Boltzmann distribution among energy levels of singly-ionized vanadium in dc glow discharge and rf inductively coupled discharge plasmas, *J. Anal. At. Spectrom.* 14 (1999) 1727–1730.
- [21] K. Wagatsuma, K. Hirokawa, Selective detection of emission lines from sputtered particles in glow discharge plasma with a modified hollow cathode lamp, *Spectrochim. Acta Part B* 43 (1988) 831–839.
- [22] K. Wagatsuma, K. Hirokawa, Emission spectroscopic studies of Grimm-type glow discharge plasma with argon–helium gas mixtures, *Spectrochim. Acta Part B* 42 (1987) 523–531.
- [23] D. Pollmann, K. Ingeneri, W.W. Harrison, Comparison of atomization and ionization in direct current, radio-frequency and microsecond pulse discharges, *J. Anal. At. Spectrom.* 11 (1996) 849–853.
- [24] S.K. Ohorodnik, W.W. Harrison, Plasma diagnostic measurements in the cryogenically cooled glow discharge, *J. Anal. At. Spectrom.* 9 (1994) 991–996.
- [25] E.S. Fishburne, Transfer of electronic energy between a metastable argon atom and a nitrogen molecule, *J. Chem. Phys.* 47 (1967) 58–63.
- [26] K. Imura, R. Midorikawa, T. Kasai, H. Ohoyama, D. Che, Observation of relative population change in the  $3P_0$  and  $3P_2$  states for Ar glow discharge formation, *Chem. Lett.* 6 (1996) 299–300.
- [27] J.F. Prince, C.B. Collins, W.W. Robertson, Spectra excited in an argon afterglow, *J. Chem. Phys.* 40 (1964) 2619–2626.
- [28] T.D. Nguyen, Rotational and vibrational distributions of  $N_2$  ( $C^3\Pi_u$ ) excited by state-selected  $Ar(^3P_2)$  and  $Ar(^3P_0)$  metastable atoms, *Chem. Phys.* 79 (1983) 41–55.
- [29] J.M. Calo, R.C. Axtmann, Cross section for the production of  $N_2$  ( $C^3\Pi_u$ ) from metastable argon atoms, *J. Chem. Phys.* 54 (1971) 4961–4963.
- [30] J.W. Coburn, E. Kay, Plasma diagnostics of an rf-sputtered glow discharge, *Appl. Phys. Lett.* 18 (1971) 435–438.
- [31] E.W. Eckstein, J.W. Coburn, E. Kay, Diagnostics of an r.f. sputtering glow discharge—correlation between atomic absorption and mass spectrometry, *Int. J. Mass Spectrom. Ion Phys.* 17 (1975) 129–138.
- [32] A. Bogaerts, R. Gijbels, Modeling of metastable argon atoms in a direct-current glow discharge, *Phys. Rev. A* 52 (1995) 3743–3751.
- [33] A. Bogaerts, R.D. Guenard, B.W. Smith, J.D. Winefordner, W.W. Harrison, R. Gijbels, Three-dimensional density profiles of argon metastable atoms in direct current glow discharge: experimental study and comparison with calculations, *Spectrochim. Acta Part B* 52 (1997) 219–229.
- [34] W. Hang, C. Baker, B.W. Smith, J.D. Winefordner, W.W. Harrison, Microsecond-pulsed glow discharge time-of-flight mass spectrometry: analytical advantages, *J. Anal. At. Spectrom.* 12 (1997) 143–149.
- [35] W.W. Harrison, W. Hang, Pulsed glow discharge time-of-flight mass spectrometry, *J. Anal. At. Spectrom.* 11 (1996) 835–840.
- [36] Y. Su, P. Yang, Z. Zhou, X. Wang, F. Li, B. Huang, J. Ren, M. Chen, H. Ma, G. Zhang, Feasibility of applying microsecond-pulse glow discharge time of flight mass spectrometry in surface depth analysis, *Spectrochim. Acta Part B* 53 (1997) 1413–1420.
- [37] D.A. Solyom, G.M. Hieftje, Advancing the capabilities of a glow-discharge sector-field mass spectrometer, *J. Anal. At. Spectrom.* 17 (2002) 329–333.
- [38] C.L. Lewis, E.S. Oxley, C.K. Pan, R.E. Steiner, F.L. King, Determination of  $^{40}Ca^+$  in the presence of  $^{40}Ar^+$ : an illustration of the utility of time-gated detection in pulsed glow discharge mass spectrometry, *Anal. Chem.* 71 (1999) 230–234.
- [39] C. Pan, F.L. King, Time-resolved studies of ionized sputtered atoms in pulsed radio frequency powered glow discharge mass spectrometry, *Anal. Chem.* 65 (1993) 3187–3193.
- [40] C. Pan, F.L. King, Ion formation processes in the afterpeak time regime of pulsed glow discharge plasmas, *J. Am. Soc. Mass Spectrom.* 4 (1993) 727–732.
- [41] F.L. King, C. Pan, Temporal signal profiles of analytical species in modulated glow discharge plasmas, *Anal. Chem.* 65 (1993) 735–739.
- [42] C. Pan, F.L. King, Direct determination of trace elements in graphite matrices using modulated glow discharge atomic absorption spectrometry, *Appl. Spectrosc.* 47 (1993) 300–304.
- [43] R.E. Steiner, C.L. Lewis, F.L. King, Time-of-flight mass spectrometry with a pulsed glow discharge ionization source, *Anal. Chem.* 69 (1997) 1715–1721.
- [44] L.A. Riseberg, W.F. Parks, L.D. Scheerer, Penning ionization of Zn and Cd by noble-gas metastable atoms, *Phys. Rev. A* 8 (1973) 1962–1968.
- [45] K. Kano, M. Suzuki, H. Akatsuka, Spectroscopic measurement of electron temperature and density in argon plasmas based on collisional-radiative model, *Plasma Sources Sci. Technol.* 9 (2000) 314–322.
- [46] T. Fujimoto, Kinetics of ionization–recombination of plasma and population density of excited ions. I. Equilibrium plasma, *J. Phys. Soc. Jpn.* 47 (1979) 265–272.

- [47] T. Fujimoto, Kinetics of ionization–recombination of plasma and population density of excited ions. IV. Recombining plasma—low temperature case, *J. Phys. Soc. Japan* 49 (1980) 1569–1576.
- [48] J.A.M. van der Mullen, Excitation equilibria in plasmas; a classification, *Phys. Rep.* 191 (1990) 109–220.
- [49] N.P. Ferreira, J.A. Strauss, H.G.C. Human, Distribution of metastable argon atoms in the modified Grimm-type electrical discharge, *Spectrochim. Acta Part B* 37 (1982) 273–279.
- [50] C. Pan, F.L. King, Atomic emission spectrometry employing a pulsed radio-frequency-powered glow discharge, *Appl. Spectrosc.* 47 (1993) 2096–2101.
- [51] G.P. Jackson, C.L. Lewis, S. Doorn, V. Majidi, F.L. King, Spatial, spectral and temporal characteristics of a millisecond-pulse glow discharge. Metastable argon atom production, *Spectrochim. Acta Part B* 56 (2001) 2449–2464.
- [52] R. Hugon, G. Henrion, M. Fabry, Time resolved determination of the electron energy distribution function in a DC pulsed plasma, *Meas. Sci. Technol.* 7 (1996) 553–559.
- [53] M. Bourene, J. Le Calve, De-excitation cross sections of metastable argon by various atoms and molecules, *J. Chem. Phys.* 58 (1973) 1452–1458.
- [54] D.W. Setser, D.H. Stedman, J.A. Coxon, Chemical applications of metastable argon atoms. IV. Excitation and relaxation of triplet states of  $N_2$ , *J. Chem. Phys.* 53 (1970) 1004–1020.
- [55] L.G. Piper, J.E. Velazco, D.W. Setser, Quenching cross sections for electronic energy transfer reactions between metastable argon atoms and noble gases and small molecules, *J. Chem. Phys.* 59 (1973) 3323–3340.
- [56] J. Le Calve, M. Bourene, Pulse radiolysis study of argon–nitrogen mixtures. Measurement of the rate constant of metastable argon de-excitation by nitrogen, *J. Chem. Phys.* 38 (1973) 1446–1451.
- [57] J.E. Velazco, J.H. Kolts, D.W. Setser, Rate constants and quenching mechanisms for the metastable states of argon, krypton, and xenon, *J. Chem. Phys.* 69 (1978) 4357–4373.
- [58] G.H. Copley, C.S. Lee, Electron excitation and deexcitation coefficients for the  $^3P_2, ^3P_1, ^3P_0, ^1P_1$  levels of argon, *Can. J. Phys.* 53 (1975) 1705–1714.
- [59] C.M. Ferreira, J. Loureiro, A. Ricard, Populations in the metastable and resonance levels of argon and stepwise ionization effects in a low-pressure argon positive column, *J. Appl. Phys.* 57 (1985) 82–90.
- [60] J.M. Calo, R.C. Axtmann, Vibrational relaxation and electronic quenching of the  $C^3\Pi_u$  ( $v'=1$ ) state of nitrogen, *J. Chem. Phys.* 54 (1971) 1332–1341.
- [61] A.W. Johnson, R.G. Fowler, Measured lifetimes of rotational and vibrational levels of electronic states of  $N_2$ , *J. Chem. Phys.* 53 (1970) 65–72.
- [62] A. Bogaerts, R. Gijbels, Modeling of a microsecond pulsed glow discharge: behavior of the argon excited levels and of the sputtered copper atoms and ions, *J. Anal. At. Spectrom.* 16 (2001) 239–249.
- [63] G.P. Jackson, Reducing Interferences in Glow Discharge Spectroscopies Using Transient Operation Collision-Induced Dissociation, Dissertation, Department of Chemistry, West Virginia University, Morgantown, 2002.
- [64] A. Bogaerts, R. Gijbels, Fundamental aspects and applications of glow discharge spectrometric techniques, *Spectrochim. Acta Part B* 53 (1998) 1–42.
- [65] K. Wagatsuma, K. Hirokawa, Quenching mechanisms in argon–nitrogen or neon–nitrogen glow discharge plasmas, *Anal. Chem.* 61 (1989) 326–329.
- [66] N.G. Adams, A.G. Dean, D. Smith, Thermal energy reactions of rare-gas atomic ions with molecular oxygen and nitrogen, *Int. J. Mass Spectrom. Ion Process.* 10 (1972) 63–76.
- [67] E.W. McDaniel, V. Cermak, A. Dalgarno, E.E. Ferguson, L. Friedman, *Ion–Molecule Reactions*, 10th ed, John Wiley & Sons, New York, 1970.
- [68] C. Kenty, The recombination of argon ions and electrons, *Phys. Rev.* 32 (1928) 624–635.
- [69] M.A. Biondi, Studies on the mechanism of electron–ion recombination. I, *Phys. Rev.* 129 (1963) 1181–1188.
- [70] K. Kano, H. Akatsuka, Numerical study of population inversion between excited states of Ar I in a recombining Ar plasma by He contact cooling, *Jpn. J. Appl. Phys.* 40 (2001) 4701–4708.
- [71] N.A. Dyatko, Y.Z. Ionikh, N.B. Kolokolov, A.V. Meshchanov, A.P. Napartovich, Jumps and bi-stabilities in electron energy distribution in Ar– $N_2$  post discharge plasma, *J. Phys. D: Appl. Phys.* 33 (2000) 2010–2018.
- [72] S.K. Dahli, Electrical characteristics of pulsed glow discharges, *IEEE Trans. Plasma Sci.* 17 (1989) 603–611.
- [73] F.M. Penning, *Physik* 46 (1925) 225.
- [74] S. Inaba, T. Goto, S. Hattori, Determination of the Penning excitation cross sections of Mg atoms by He, Ne, and Ar metastable atoms, *J. Phys. Soc. Jpn.* 52 (1983) 1164–1167.
- [75] D.R. Lide, in: D.R. Lide (Ed.), *CRC Handbook of Chemistry and Physics*, CRC Press, New York, 2000. pp. 10-175–10-176.
- [76] M. Hecq, A. Hecq, Presence of doubly-ionized metal ions in rare gas glow discharges, *J. Appl. Phys.* 56 (1984) 872–873.
- [77] W. Vieth, J.C. Huneke, Studies on ion formation in a glow discharge mass spectrometry ion source, *Spectrochim. Acta Part B* 45 (1990) 941–949.
- [78] D. Fang, R.K. Marcus, Effect of discharge conditions and cathode identity on charged particle populations in the negative glow region of a simple diode discharge, *Spectrochim. Acta Part B* 46 (1991) 983–1000.
- [79] N.P. Ferreira, H.G.C. Human, L.R.P. Butler, Kinetic temperatures and electron densities in the plasma of a side view Grimm-type glow discharge, *Spectrochim. Acta Part B* 35 (1980) 287–295.

- [80] N.P. Ferreira, H.G.C. Human, A study of the density of sputtered atoms in the plasma of the modified Grimm-type glow discharge source, *Spectrochim. Acta Part B* 36 (1981) 215–229.
- [81] N. Jacubowski, I. Feldmann, D. Steuwer, Grimm-type glow discharge ion source for operation with a high resolution inductively coupled plasma mass spectrometry instrument, *J. Anal. At. Spectrom.* 12 (1997) 151–157.
- [82] E.B.M. Steers, R.J. Fielding, Charge-transfer excitation processes in the Grimm lamp, *J. Anal. At. Spectrom.* 2 (1987) 239–244.
- [83] K. Wagatsuma, K. Hirokawa, Spectroscopic studies of excitation mechanisms on singly-ionized copper emission lines in Grimm-type glow discharge plasmas with helium mixture technique, *Spectrochim. Acta Part B* 46 (1991) 269–281.
- [84] K. Wagatsuma, H. Matsuta, Control of d.c. bias current in radio-frequency glow discharge source and its emission characteristics, *Spectrochim. Acta Part B* 54 (1999) 527–535.
- [85] C. Yang, K. Ingeneri, W.W. Harrison, A pulsed Grimm glow discharge as an atomic emission source, *J. Anal. At. Spectrom.* 14 (1999) 693–698.
- [86] C. Yang, W.W. Harrison, Investigation of a novel hollow cathode configuration for Grimm-type glow discharge emission, *Spectrochim. Acta Part B* 56 (2001) 1195–1208.
- [87] S. Caroli, The hollow cathode emission source: a survey of the past and a look into the future, *Prog. Anal. At. Spectrosc.* 6 (1983) 253–292.
- [88] R.K. Marcus, F.L. King, W.W. Harrison, Hollow cathode plume as an atomization/ionization source for solids analysis, *Anal. Chem.* 58 (1986) 972–974.
- [89] C.L. Chakrabarti, K.L. Headrick, J.C. Hutton, Z. Bicheng, P.C. Bertels, M.H. Back, Pulsed and transient modes of atomization by cathodic sputtering in a glow discharge for atomic absorption spectrometry, *Anal. Chem.* 62 (1990) 574–586.
- [90] R.L. Smith, D. Serxner, K.R. Hess, Assessment of the relative role of penning ionization in low-pressure glow discharges, *Anal. Chem.* 61 (1989) 1103–1108.
- [91] M.K. Levy, D. Serxner, A.D. Angstadt, R.L. Smith, K.R. Hess, Optical investigations of excitation processes responsible for ionized sputtered species in a low pressure, low current, coaxial geometry glow discharge, *Spectrochim. Acta Part B* 46 (1991) 253–267.
- [92] J.E. Parker, R.S. Lehle, Ion–molecule reactions, *Int. J. Mass Spectrom. Ion Phys.* 7 (1971) 421–469.
- [93] X. Yan, K. Ingeneri, W. Hang, W.W. Harrison, Factors influencing signal profiles in microsecond pulsed glow discharge atomic emission spectrometry, *J. Anal. At. Spectrom.* 16 (2001) 819–824.
- [94] J.M. Brackett, J.C. Mitchell, T.J. Vickers, Temperature and electron density measurements in a DC glow discharge, *Appl. Spectrosc.* 38 (1984) 136–140.
- [95] C.V. Dijk, B.W. Smith, J.D. Winefordner, Spatial and temporal studies of a glow discharge, *Spectrochim. Acta Part B* 37 (1982) 759–768.
- [96] D.M. Mehs, T.M. Niemczyk, Excitation temperatures in the hollow cathode discharge, *Appl. Spectrosc.* 35 (1981) 66–69.
- [97] A. Bogaerts, R. Gijbels, Fundamental aspects and applications of glow discharge spectrometric techniques, *Spectrochim. Acta Part B* 53 (1998) 1–42.
- [98] C.L. Lewis, Characterization and Applications of Pulsed Millisecond Glow Discharge Sources, Dissertation, Department of Chemistry, West Virginia University, Morgantown, 2001, p. 161.
- [99] C.L. Lewis, G.P. Jackson, S.K. Doorn, V. Majidi, F.L. King, Spectral, spatial and temporal diagnostics of a millisecond-pulse glow discharge: copper atom and ion production, *Spectrochim. Acta Part B* 56 (2001) 487–501.
- [100] E.D. Klema, J.S. Allen, Drift velocities of electrons in argon, nitrogen, and argon–nitrogen mixtures, *Phys. Rev.* 77 (1950) 661–665.
- [101] L. Colli, U. Facchini, Drift velocity of electrons in argon, *Rev. Sci. Instrum.* 23 (1952) 39–42.
- [102] R.A. Nielson, Absolute values of the electron drift velocity in nitrogen, helium, neon and argon, *Phys. Rev.* 50 (1936) 950–954.
- [103] R.S. Mason, P.D. Miller, I.P. Mortimer, Anomalous loss of ionization in argon–hydrogen plasma studied by fast flow glow discharge mass spectrometry, *Phys. Rev. E* 55 (1997) 7462–7472.
- [104] P.F. Knewstubb, A.W. Tickner, Mass spectrometry of ions in glow discharges. I. Apparatus and its application to the positive column in rare gases, *J. Chem. Phys.* 36 (1962) 674–683.
- [105] S.G. Lias, J.F. Liebman, R.D. Levin, Evaluated gas phase basicities and proton affinities of molecules; heats of formation of protonated molecules, *J. Phys. Chem. Ref. Data* 13 (1984) 695–808.
- [106] T. Su, M.T. Bowers, Ion–polar molecule collisions: the effect of size on ion–polar molecule rate constants; the parameterization of the average-dipole-orientation theory, *Int. J. Mass Spectrom. Ion Phys.* 12 (1973) 347–356.